1-1-2013

Experimental Study On Piping Failure of Earthen Levee and Dams

Yusuf Ahmed Sharif
University of South Carolina - Columbia

Experimental Study on Piping Failure of Earthen Levee And Dams

by

Yusuf Ahmed Sharif

Bachelor of Science
Bangladesh University of Engineering and Technology, 2002

Master of Science
Bangladesh University of Engineering and Technology, 2006

Submitted in Partial Fulfillment of the Requirements

for the Degree of Doctor of Philosophy in

Civil Engineering

College of Engineering and Computing

University of South Carolina

2013

Accepted by:

M. Hanif Chaudhry, Major Professor

Jasim Imran, Committee Member

Enrica Viparelli, Committee Member

Jamil A Khan, Committee Member

Lacy Ford, Vice Provost and Dean of Graduate Studies

Acknowledgments

I would like to express my appreciation and thanks to the major advisor of my dissertation Prof. M. Hanif Chaudhry, for his guidance and suggestions throughout the study. Special thanks to the co-advisor of the dissertation Dr. Jasim Imran for his suggestions and comments. Special thanks are also extended to my committee members, Drs. Jamil Khan and Enrica Viparelli. I would also like to specially thank Dr.Mohamed Elkholy for his collaboration in the research work and Tyler Wyatt(Final year geology student at USC) who really worked hard helping me building these levees for my experiments. I am also thankful to Dr. Pranab Mahapatra for his guidance and help. I would like to give special thanks to my father-in-law, Dr. Abdul Malek Miah, mother-in-law Mrs. Meherunnesa Begum and my wife Rudia Begum for their continuous encouragement throughout my studies. I would also like to remember the blessings of my late parents Dr. H. S. Faruque and Mrs. Rosy Sharif. And the great thanks are due to my CREATOR.

Abstract

Piping in an earthen levee, one of the main causes of failure, is a complex phenomenon. Most of the available research on piping failure has been on non-cohesive sandy soils. Jet Erosion Test and Hole Erosion Test have been conducted to study piping failure in an indirect manner. However, no general purpose formula is presently available to describe the erosion process due to complex erosion characteristics of cohesive soils in earthen levees.

Experimental investigations in a flume to understand the piping erosion process in an earthen levee are conducted in this research. One of the sidewalls and the bottom of the flume is built with transparent plexiglass. A side weir is used to maintain a nearly-constant upstream water level. Tests are done with a mixture of sand, silt and clay with different compaction rates. Image processing technique is applied to track the erosion process, both from the side and the bottom. The erosion process is initiated on the upstream side of the levee by removing an embedded plug. The effect of the compaction on the change in the depth, the area and the volume of erosion during the piping phenomenon are studied. Empirical equations to estimate the depth of erosion, side area of the piping zone and volume of eroded material are presented for the same soil mixture but with different compaction rate. The volume of erosion is calculated using image processing data from side and bottom views and from side views only. The former gives a more accurate estimate.

Using different mixtures of sand, silt and clay show that a minor change in the clay

percentage in the soil mixtures significantly affects the time required for erosion. The ratio of the average depth of erosion to the average bottom width of piping remains approximately 1 during the erosion process. Empirical relation to estimate the depth of erosion as a function of time and the coefficient of soil erodibility for different soil mixtures with the same compaction is presented.

A one-dimensional numerical model to predict the evolution of the internal erosion in an earthen embankment is developed. The numerical model can predict the depth of erosion along the piping zone. The numerical model solves the Exner equation to predict the development of erosion depth with time. The model is used to analyze the upstream and downstream slope, the crest width, the initial upstream water depth and the initial piping diameter on the internal erosion process.

Table of Contents

List of Tables

List of Figures

Chapter 1

Introduction

1.1 Background

A levee is an artificial water barrier, typically constructed to prevent flooding by placing and compacting a mixture of soil, sand, clay and/or rock since the early days of civilization.

Large mounds of earth have been used to block rivers to provide water to nearby towns and to the irrigation fields and levees along riverbanks have been constructed to protect populated areas from flooding. Some of the largest dams in the world are earth embankments. The United States Committee on Large Dams (USCOLD) estimates that nearly 80% of all large dams in the world are currently in operation in the United States alone, and about 11000 flood control and multipurpose dams were constructed with assistance from the United States government (Caldwell, 1999). Earthen levees are cheaper to construct and commonly constructed from locally available material. The Mississippi levee system represents one of the largest such systems found anywhere in the world. It comprises over 3,500 miles (5,600 km) of levees extending some 1,000 kilometres (620 mi) along the Mississippi, stretching from Cape Girardeau, Missouri, to the Mississippi Delta. They were begun by French settlers in Louisiana in the 18th century to protect the city of New Orleans. The first Louisiana levees were about 3 feet (0.91 m) high and covered a distance of about 50 miles (80 km) along the riverside. The U.S. Army Corps of Engineers, in conjunction with the

Mississippi River Commission, extended the levee system beginning in 1882 to cover the riverbanks from Cairo, Illinois to the mouth of the Mississippi delta in Louisiana. By the mid-1980s, they had reached their present extent and averaged 24 feet (7.3 m) in height; some Mississippi levees are as high as 50 feet (15 m). The Mississippi levees also include some of the longest continuous individual levees in the world. One such levee extends southwards from Pine Bluff, Arkansas, for a distance of some 380 miles (610 km). There is the failure and the inherent risks to people, land and property in downstream the levee from the flood wave indicates importance of the design and construction.

An increase in runoff increases the risk of levee failure. Increased flow due to urban development is thought to be the leading cause of the March 26, 2009 failure of the Situ Gintung Lake Dam near Jakarta in Indonesia which killed almost 100 people after heavy rains caused the dam to fail (BBC, 2009; Jakarta Post, 2009).

The 1976 Teton dam failure in Idaho due to piping; 14 people were killed and there was over $1 billion in damages (Solava and Delatte, 1995). Dam failures may result in loss of life in addition to huge ecological damage. In 1998, when Aznacollar tailing pond dam failed in Spain, a large amount of toxic material spilled into the river system (Eriksson and Adamek, 2000). Levee failures depend upon the type of structure, their configuration material used for the construction, impacting forces and other environmental factors. A levee is likely to fail gradually because of erosion of its materials by water flow or by wave action involving mixed-regime flow, strong sediment transport, and rapid morphological changes. Levee breach processes are complex and involves complex interactions among soil, water, and structure.

The major causes of earthen levee failure are overtopping, foundation and struc-

tural defects, and piping. According to Costa (1985), 28% of earthen embankment failures are caused by piping. Piping failure or internal erosion is the process by which seepage results in the removal of fines along a path between the upstream and downstream faces of the levee. Larger sediment particles are washed out by a process known as backward erosion ultimately leading to the formation of a pipe or tunnel carrying a significant amount of discharge. The pipe increases in diameter by the removal of material at the wall primarily attributable to shear forces until slumping of the roof or local collapse occurs. The Teton dam failure is a classic example of piping failure (Ponce 1982). Some case studies have shown that the pipe initiation and erosion stages may take upto several days or weeks, whereas the subsequent levee breaching may take only a few hours or less. Piping may occur because of seepage or leakage flow through weak layers, desiccation cracks, structural joints, dead tree roots, and animal burrows in the levee (Safety of dams and reservoirs act-DNR).

1.2 Problem Statement

The difficulty associated with parameterization of piping failure arises due to the incomplete understanding of the erosion mechanism of cohesive soil and the large number of factors upon which it depends. Experimental study of piping failure has been limited due to difficulty in visualizing the process.

The dominating factors controlling erosion mechanism depend on various geotechnical properties of soil. Cohesive soils contain fine-grained particles, like silt and clay. So, erodibility criteria of the soil is very important for defining the complex behavior of piping failure. And the erodibility of soil depends on geotechnical factors, such as compaction of soil, optimum water content of soil, erodible coefficient of soil, etc. Therefore, it is important to know the geotechnical parameters and their interdependence for the prediction of piping failure properly.

1.3 Research Objectives

The primary objective of this work is to study failure of earthen levee by piping under controlled conditions, i.e. continuous fow, constant upstream head and soil compaction. Developing new methodology to observe and measure piping erosion is one of the major objectives. Experiments are conducted in the Hydraulics Laboratory, University of South Carolina (USC). The present study has two major focuses: (i) effect of compaction on erosion process of earthen levee and, (ii) effect of soil composition on piping failure of levee.
Developing new methodology to observe and measure piping erosion is one of the major objectives.

1.4 Methodology

The two main objectives discussed previously are achieved through different sets of laboratory experiments. For the first objective, to observe and quantify the erosion process, a set of experiments are conducted in a laboratory flume on a soil mixture using different compaction rates. By using the experimental results, a general relationship is developed to estimate the rate of erosion in a non-dimensional form as a function of time and the rate of compaction.

For the second objective of developing a new methodology to determine erodibility coefficient for different mixtures, experiments with the same compaction rate are performed on different soil mixtures. Each experiment is continued until predefined criteria are satisfied. The experimental results are analyzed and compared to the results available in the literature.

Finally, the experimental work has been validated with a one dimensional numeri-

cal work. A one-dimensional numerical model to predict the evolution of the internal erosion in an earthen embankment is developed.

1.5 Dissertation Outline

Chapter 1 presents a general discussion of piping failure in a levee and associated problems, the study objectives, methodology and dissertation outline.

Chapter 2 has two parts: the first part presents a literature review on the internal erosion and piping failure of earthen levee, both in laboratory and at large scales, while the second part is a literature review on erodibility coefficient and initial critial shear stress of soil.

In chapter 3, a general description of the experimental procedures and setup to study piping failure in a laboratory flume are outlined.

Chapter 4 presents the non-dimesional analysis for the effect of compaction on the erosion process in earthen levee. The chapter also defines a new non-dimensional quantitative formula to estimate the depth, area and volume of eroded soil from the piping zone of the earthen levee.

Chapter 5 presents the results of depths of erosion with time for different soil mixtures on the erosion process in an earthen levee and trials are made to estimate the erosion coefficient. A comparison between the experimental results and other available methods in the literature is also given.

Chapter 6 presents the validation of experimental work for results of depths of erosion with time for different compaction in same soil mixtures and same compaction

in different soil mixtures to the numerical model and the model can also predict result of depth of erosion for different conditions in the levee like as change in crest width, upstream and downstream slopes.

The summary and conclusions drawn from the results of the study and recommendations are presented in Chapter 7.

Chapter 2

Literature Review

The literature review is divided into two sections: erosion of cohesive soil and the coefficient of soil erodibility. The first section focuses on the erosion process of cohesive soil with different compaction rates and the second section reviews the Jet and Hole Erosion test for determining the coefficient of soil erodibility.

2.1 Piping Failure of Earthen Embankment

Earthen embankments are built from soil with different percentages of sand, silt and clay. The erosion process may vary depending on the proportion of the soil composition and the optimum water content.

Overtopping and piping are the two common causes of the failure of earthen embankments. Dam failures due to overtopping have been studied by many researchers but the studies on piping failure are limited. The failure of an embankment depends on many factors: geometry of the structure, erodibility of the soil, upstream water head and the hydraulic gradient, soil gradation and degree of compaction during construction. The soil properties are one of the major factors affecting the failure of embankments. Porosity has a major effect on the percolation and seepage of water in the embankment and can be reduced with proper compaction during construction. A couple of experimental parametric studies related to suffusion and backward erosion measured the erodibility of soil materials and the erosion of noncohesive compacted soil. Several methods, both field and laboratory are developed for characterizing

earthen material erodibility, including flume tests (Shaikh et al., 1988), channel tests (Arulanandan and Perry, 1983), rotating cylinders (Chapuis, 1986; Chapuis and Gatien, 1986), hole erosion tests (Maranha das Neves, 1989; Reddi et al., 2000), slot tests (Wan and Fell, 2004a), jet erosion test (Hanson, 1991; Hanson and Robinson, 1993; Hanson et al., 2010).

Foster et al. (2000b,a) stated that internal erosion and piping have historically resulted in about 0.5% (1 in 200) embankment failure, and 1.5%(1 in 60) experiencing a piping incident. Internal erosion occurs due to the transport and migration of soil particles within the structure. Understanding the internal erosion mechanism is difficult due to its complexity and due to the difficulties for their detection. With internal erosion, the hydraulic and mechanical characteristics of the soil are altered. The material permeability, for instance, may significantly change. This may increase the pore pressure, which may contribute to the stability of the slopes of the structure (Bendahmane et al., 2008). A series of four large scale, earthen embankment internal erosion tests have been conducted at the USDA-ARS Hydraulic Engineering Research Unit in Stillwater, Oklahoma (Hanson et al., 2010) to evaluate how soil properties influence the erosion rate, timing and geometry of an embankment breach as well as outflow from an embankment breach. Fell et al. (2003) have provided a framework to estimate the time for the initiation of piping and enlarging the hole until the breach. The Teton dam failure is a classic case of piping failure (Seed and Duncan, 1981). Breach formation was thoroughly investigated by the IMPACT project, funded by European Commission (Morris et al., 2007).

Vaskinn et al. (2004) conducted field tests on rock fill, clay and moraine embankments. Two different trigger mechanisms were used to initiate the internal erosion by two 200 mm diameter pipes. They found that the rate and mechanisms of failure

were typically more resistant compared to the values given by the existing analyses and guidelines.

Briaud (2008), based on erosion resistance categories proposed that the rate of erosion is different for different soils. Briaud (2008) also reported that compaction effort is more significant for some soils. Wan and Fell (2004) indicated that erosion rate index of soil is strongly influenced by the degree of compaction.

Awal et al. (2011) recently studied piping failure of a dam in a sloping flume at Kyoto University. They found that the lake water level, initial size of the pipe, lake water volume, location of the pipe and slope significantly affect the outflow hydrograph and peak discharge. A full scale experiment on the levee failure was conducted in the Netherlands with pure sand of different grain sizes in which erosion resulted in the formation of a piping channel leading to significant deformation and failure of the levee (van Beek et al., 2010). Several other tests were done to measure piping failure, e.g., true triaxial piping test apparatus for the evaluation of piping potential in earth structures (Richards and Reddy, 2010), laboratory tests on the rate of piping erosion of soils in embankment dams (Wan and Fell, 2004a), influence of porosity on piping models of levee failure (Ojha et al., 2001).

2.2 Erodibility Coefficient

The erodibility of the soil determines the time for the embankment to collapse and it is an essential parameter for predicting the embankment performance for internal erosion failure. Bonelli et al. (2010) estimated the rates of erosion from Hole erosion test (HET) and quantified the embankment piping failure time in an indirect method. As different soils erode at different rates, they attempted to correlate critical stress and coefficient of erosion to the common geotechnical soil properties but no empirical

relationship have been developed from their work. A number of numerical procedures have been developed to predict the time for piping failure (Alamdari et al., 2012; Lachouette et al., 2008). To summarize, the physical processes involved in the piping failure are complex and the details of the mechanism of the dam failures by piping are still lacking. To the authors' knowledge, evolution of piping width, depth, and volume with time has not been studied experimentally so far.

2.3 JET Erosion Test

Jet index method provides a standard method of expressing the erosion resistance to assist those working with different soils and soil conditions to measure the erosion resistance for design purposes. It provides a common system of characterizing soil properties to develop performance and prediction relationships. Jet erosion test cannot be used for determining the erodibility of the soil if it has structural characteristics larger than the jet testing device. It has to be observed that the test sample and the test are representative of the expected conditions at the site. If the soil is saturated prior to an erosion event, then the soil must be tested in that particular condition. Because at present the effect of water chemistry on detachment rate is unknown, water quality should be simulated during testing close to the water quality anticipated during actual erosion.

2.4 Hole Erosion Test

Hole Erosion Test (HET) is a laboratory test where piping erosion is simulated on a small scale by passing flow through a pre-drilled hole in a test specimen. The hydraulic gradient required to cause progressive erosion and enlargement of the pre-drilled hole is used to compute the threshold shear stress for piping erosion of the material. The increase in the flow rate during progressive erosion of the drilled hole

is used to determine the erosion rate coefficient. This is a key parameter to indicate how quickly a piping erosion may proceed when the threshold for erosion is exceeded. The rate coefficient varies over several orders of magnitude from geotechnical considerations. Therefore, a second parameter, the Erosion Rate Index is computed.

The averaged k_d values obtained from JET (Jet Erosion Test) tests conducted in-situ are 0.98 m^3/t.s for soil material (64% sand, 29% silt and 7% clay) which is expected to exhibit very rapid erosion and 0.00029 m^3/t.s for soil material (25% sand, 49% silt and 26% clay) which is expected to exhibit very slow erosion.

Wan and Fell (2004a) tested 13 soil samples to relate the erosion properties with the other soil properties. They found it more convenient to use the erosion rate index, I which is defined as $I = -\log(k_d \rho_d)$, where ρ_d is the dry density of the soil. I has a range of 0 to 6 which is highly influenced by the compaction parameters (water content and dry density) of the soil. Smaller values of I implies more rapidly erodible soils. They found good correlation for I values corresponding to 95% compaction and near optimum water content from both the SET (Slot Erosion Test) and the HET (Hole Erosion Test) Tests. They introduced two formulas for calculating the erosion rate index for coarse and fine grained soils.

Recently, Bonelli et al. (2010) estimated the rates of erosion from Hole erosion test (HET) and quantified the embankment piping failure time in an indirect method. As different soils erode at different rates, they attempted to correlate critical stress and coefficient of erosion to the common geotechnical soil properties but no formulae have been developed from their work. Thoman and Niezgoda (2008) introduced a new formula for calculating the critical shear stress for cohesive soil sampled from 25 reaches along Powder River Basin in Wyoming. They found that the five soil prop-

erties on which the critical shear stress depends are: activity of the soil, dispersion ratio, specific gravity, the pH of the soil and the water content.

Regazzoni et al. (2008) compared HET and JET and found that the computed values for k_d with the JET are 3 to 80 times higher than that from HET tests. Also, they found that the critical shear stresses computed from JET are 20 to 100 times smaller than that from HET. Wahl (2010) emphasized the proper selection of the test method and the erosion mechanisms that best fit the application. Presently, the JET has been applied mostly to levee breach experiments by overtopping while HET has been applied to problems with internal erosion. Because of the discrepancy between JET and HET results, Marot et al. (2011) proposed a new erosion resistance index by linking the expended energy to the erosion phenomenon. They found that comparing the position of each soil on the I-chart shows identical erodibility classification from the two tests.

To summarize, the physical processes involved in the piping failure are complex and the details of the mechanism of the levee failures by piping are still not completely understood.

Chapter 3

Experimental Set-up and Procedures

In the present study, two different sets of experiments are performed. The first set consists of earthen embankment piping failure tests using different number of compaction rates. The second test involves the same number of compaction rates for different soil mixtures. In this chapter, a general description of the experimental setup for each set of experiments, their accuracy, and methods for data analysis are discussed.

3.1 Laboratory Flume

Experiments on the piping erosion process in an earthen levee are conducted in 6.1 m long, 0.46 m wide and 0.25 m deep wooden flume in the Hydraulic Laboratory, University of South Carolina. The 40 mm thick walls of the flume are strong enough to withstand the compaction of the soil material. The flume has a flow straightener on the upstream side to straighten the flow and reduce turbulence followed by a wave suppressor to reduce the water surface disturbances. To maintain a constant upstream water level during the experiment, a 0.30 m wide side weir, is placed with a crest elevation of 0.13 m from the bed level of the flume and is located after the wave suppressor. The weir keeps the upstream water level constant during the experiment. One of the sidewalls and bottom of a 2-m section of the flume are made of plexiglass to visualize the erosion process in the earthen embankment. A grid is marked on the side and bottom glass with 50 mm grid interval. A tank at the upstream side of the flume equipped with a 8.5 l/s pump to deliver continuous flow to the flume and a

control valve are used to regulate the flow from the pump to the flume. A collector bin is placed beside the side weir to collect the overflowing water. Figure 3.1 shows the schematic of the experimental setup.

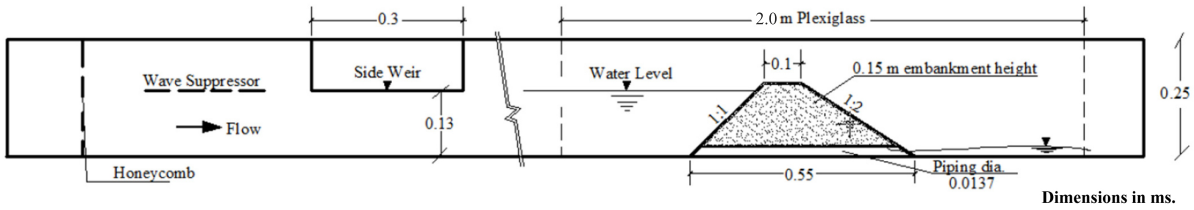

Figure 3.1: Embankment setup.

3.2 Procedure

A concrete mixture machine is used to prepare the soil mixture for building the levee. Small quantities of sand, silt and clay are poured in the tumbler of the mixture machine and rolled for 5 min to have a homogenous mixture. After adding the required amount of the soil, the optimum water content for the mixture determined by the standard proctor test is added to the soil. Then, the mixture is sieved with a sieving tray to avoid any clotting of the material due to the presence of clay in the mixture. The building process starts right after the preparation of the mixture so that the water content in the mixture does not change. Before pouring the soil mixture, a plastic pipe with a diameter, d_{in}, = 13.7 mm is placed at the side of the plexiglass wall. The material is then poured into the flume layer by layer, each layer having a maximum of six sections. Each layer has an initial height of 0.10 m and then each section is compacted with a 7.45 kg (0.25 m $\times$ 0.25 m) rammer and specified number of blows, n_b. The layer has a final height of 0.05 m. Then, a second layer is poured with an initial height of 0.1 m and compacted with the rammer and the same as for the top layer. A release height for the rammer from the surface of the layer is kept constant at 0.05 m.

The excess part from the build up material is cut down and trimmed to obtain the required slope of the levee. The levee has 1:1 slope on the upstream side and 1:2 slope on the downstream side. After trimming the levee, the plastic pipe is carefully removed and replaced by a trigger 50 mm in length to fill the 13.7 mm hole. The final levee is 0.55 m long, 0.46 m wide and 0.15 m high.

The upstream reservoir is then filled with water to 0.13 m depth. Once filled, the trigger is pulled to start the experiment. During the experiment, there is continuous inflow into the upstream reservoir. The experiment is stopped when the water level drops to less than 90% of the initial height. It is assumed that the water level is constant during the experiment with a maximum change of 10%. The eroded material is collected from the area downstream of the levee to determine the total volume eroded during the experiment.

3.3 Measurements (Image Processing)

Two high definition video cameras (SONY HDR-XR160) with 60 frames/second are used to record the erosion process from the bottom and the side of the flume.

The videos for the erosion process recorded by the side and the bottom cameras are splitted in single frames. A software based on DPTV (Digital Particle Tracking velocimetry) technique developed in-house is used to track the boundaries of the eroded area from each frame. The first step is to define the point edges of the embankment in the figure to delineate the boundary where the procedure takes place. Then, a Sobel edge detection algorithm (Jähne, 1997; Gonzalez et al., 2009) is applied

by filtering the image with the following mask:

$$G = \begin{pmatrix} -\alpha & -2\alpha & -\alpha \\ 0 & 0 & 0 \\ \alpha & 2\alpha & \alpha \end{pmatrix} \tag{3.1}$$

where, $\alpha \geq 1$. This algorithm detects the horizontal lines and ignores the vertical lines in the image. Fig. 3.2 shows the first estimate of the erosion line. The points with the highest magnitude across the width of the horizontal line is selected to represent the final bathymetry of the erosion line to the nearest $\pm$ 1 mm. Missing points on the ends are extrapolated to the boundaries to have an erosion line that fully extends from the upstream edge to the downstream one.

Figure 3.3 shows the result of delineating the boundaries of the piping zone at different time intervals. As can be seen from the figure, the maximum depth of erosion is at the inlet of the piping zone and the average depth increases with time. The water in the piping zone is under pressure except for the last 50 mm where the water is detached from the top erosion line in the embankment.

(a) Original image

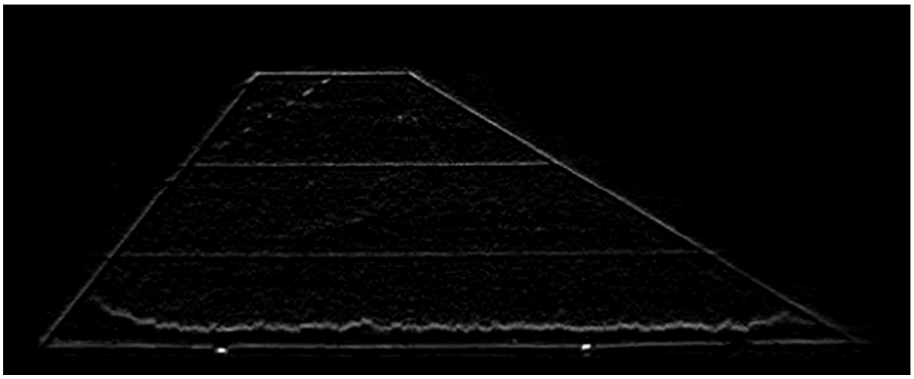

(b) After applying Sobel detector

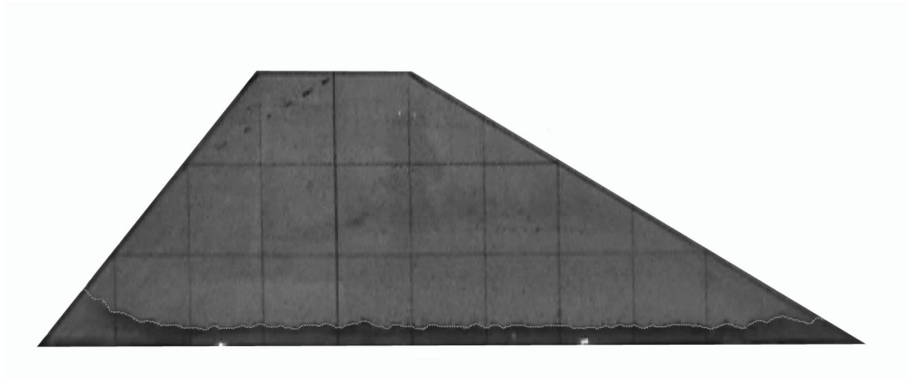

(c) Final image

Figure 3.2: Steps for Image processing.

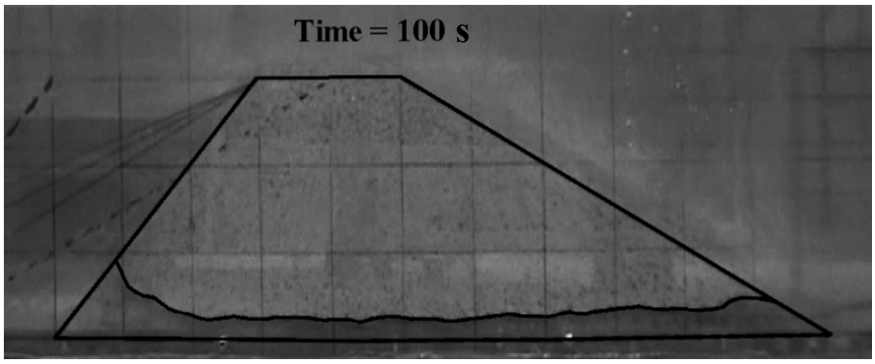

(a) $t = 100$ s

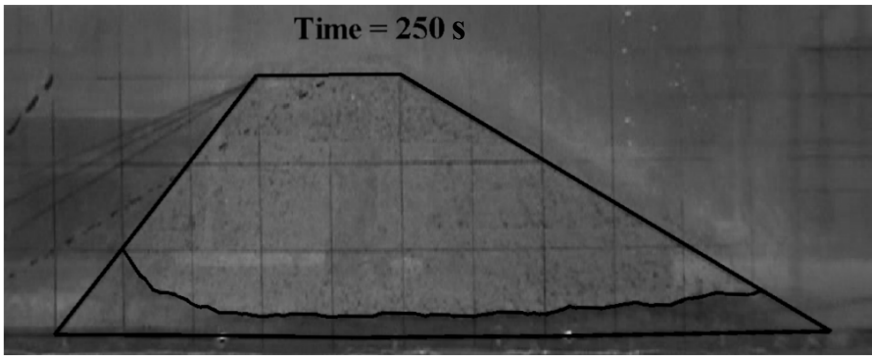

(b) $t = 250$ s

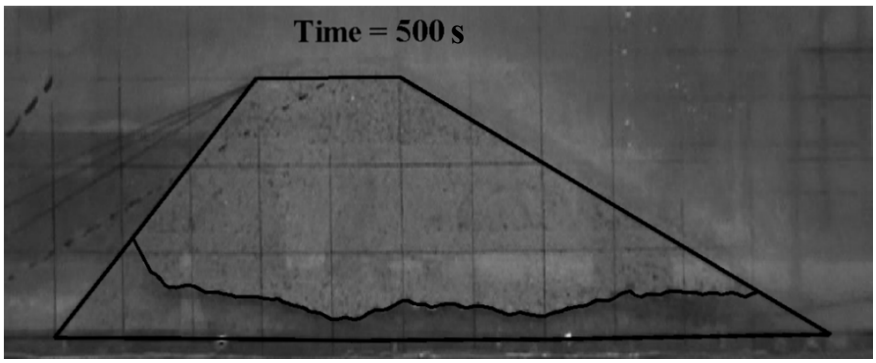

(c) $t = 500$ s

Figure 3.3: Delineation of piping zone boundaries at different time interval.

Chapter 4

Effect of Compaction

4.1 Introduction

In this set of experiments, a particular texture of the soil is used. Soil texture is a qualitative classification tool used in both the field and the laboratory to determine the class for agricultural soils classification, based on their physical texture. The classes are distinguished in the field by the "textural feel" which can be further clarified by separating the relative proportions of sand, silt and clay using grading sieves: The Particle Size Distribution (PSD). The class is a qualitative rather than a quantitative tool. It is fast, simple and effective means to assess the soils physical characteristics. USDA system uses 12 classes. In the United States, the smallest particles are clay particles and are classified by the USDA, having diameters of less than 0.002 mm. The next smallest particles are silt particles and have diameters between 0.002 mm and 0.05 mm. The largest particles are sand particles and are larger than 0.05 mm in diameter. Furthermore, large sand particles can be described as coarse, intermediate as medium, and the small as fine. The selected soil for the experiment falls into SM (sandy loam) category according to USDA chart.

Standard proctor tests are conducted to determine the maximum dry density and optimum water content of the selected soil. The term Proctor is in honor of R.R. Proctor, who in 1933 showed that the dry density of a soil for a given compactive effort depends on the amount of water that soil contains during the soil compaction.

The proctor test , ASTM D698 uses a 100 mm mould which holds 1/30 th cubic foot of soil. Compaction is conducted in three separate lifts of soil using 25 blows by a 5.5lb hammer falling 12 inches.

The sand cone test method (ASTM D1556) is used for the determination of the in-situ density and unit weight of soil. This test method is not suitable for organic, saturated or highly plastic soils that would deform or compress during the excavation of the test hole.

4.2 Methodology

The soil mixture used in this set of experiments to study the piping failure contains 64% medium sand, 29% silt (sil-co-sil 106 manufactured by US Silica) and 7% Kaolinite clay. According to USDA soil texture, the mixture is classified as sandy loam. Sandy loam soil is referred to as “select fill" due to the compaction capabilities and stability. The erosion process for this soil is categorized as “extremely rapid" (Hanson et al. (2010)). The cohesion, c, of the soil mixture measured by direct shear test is found to be 32.79 kPA and the angle of internal friction $\phi_{\text{soil}} = 32^0$. The optimum water content is determined from the standard proctor test as 9% and the corresponding maximum dry unit weight is 20.5 kN/m^3.

A total of 34.1 kg of the mixture in the first layer, 22.72 kg in the second one and 12.27 kg in the top layer is used.

Tests are done with different number of blows per section with n_b varying from as low as 5 blows/section up to 35 blows/section based on the initial trials. The relationship between the number of blows, n_b and the ratio of the dry density of the mixture obtained from sand−cone test, γ_{dry} to the maximum dry density, $\gamma_{\text{dry}_{\text{max}}}$

obtained from the proctor test is $n_b = 98.2\left(\gamma_{\text{dry}}/\gamma_{\text{dry}_{\text{max}}}\right)^{4.84}$ with r-squared value equal to 0.89.

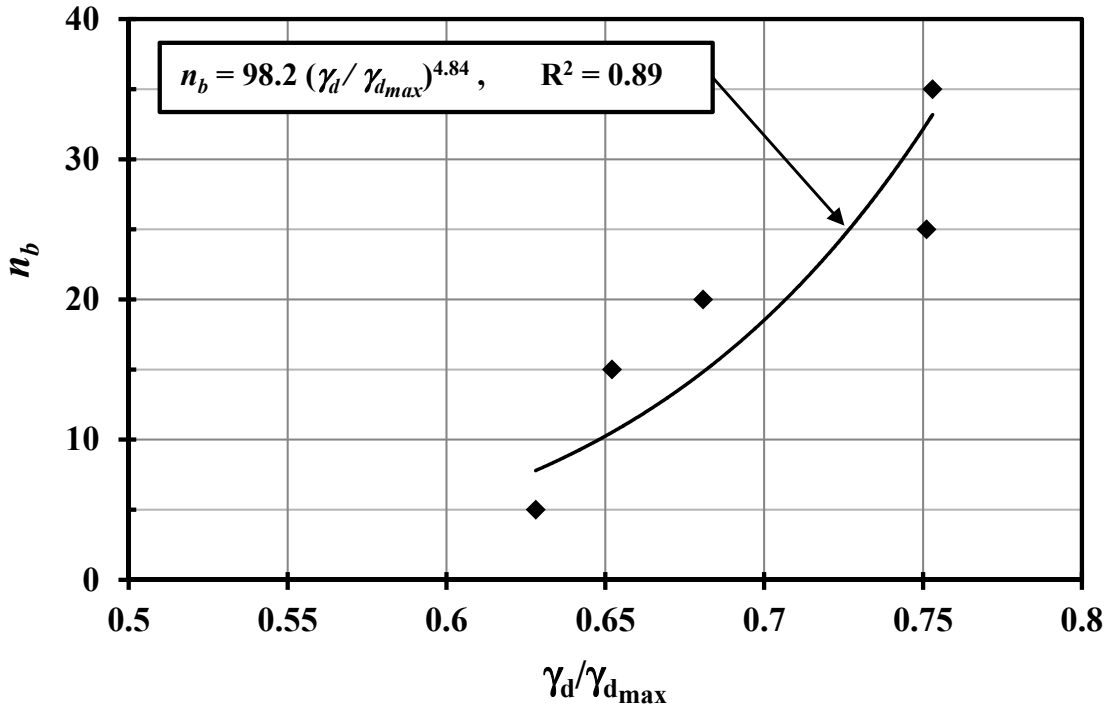

Figure 4.1: Plot of number of blows to ratio of (Dry Density/Max. Dry Density).

In the following paragraphs, the repeatability and symmetry of the erosion process are presented, followed by a discussion of the results.

4.3 Repeatability and Symmetry

Repeatability needs to be confirmed to proceed with the experiment because of the uncertainty in the behavior of soil. Multiple trials are done and care is taken in preparing the soil mixture and in compacting it. Figure 4.2a shows a comparison of four different runs for the case of $n_b = 25$ blows/section. In this figure, the x-axis represents the non-dimensional time, t/t_f, where, t is the actual time in seconds and t_f is the run time, i.e., the time taken for the water surface elevation to drop from 0.13 to 0.11 m and the y-axis represents the non-dimensional average erosion depth,

Z_{av}/H_w, where Z_{av} is the average depth of the piping zone and H_w is the initial depth of water which is equal to 0.13 m.

An experiment is conducted to check the symmetry of the flow. The pipe is placed in the center of the flume at the bed level. Only one camera located at the bottom of the flume is used. Figure 4.2b shows the original image from the bottom view and Fig. 4.2c shows the ratio of the eroded width, y, to the width of the flume, B, for both the top and the bottom line. It can be seen from the figure that the flow is symmetric about the axis of the flume with R-square value of 0.86 and also proves that placing the pipe on one side of the flume should have the same effect as placing it in the middle of the flume, as long as the friction between the glass side and the soil mixture can be neglected.

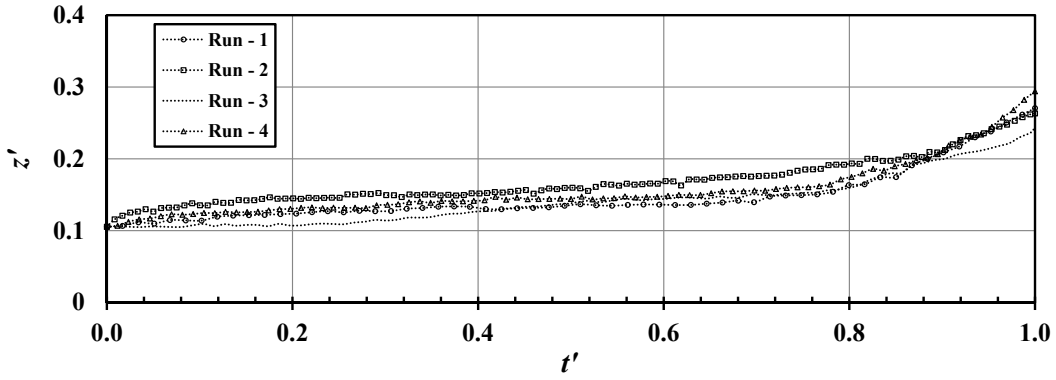

(a) Non-dimensional depth verses time for four different runs.

Figure 4.2: Repeatability and Symmetry of the erosion process.

4.4 Results

Plots are done for the change in the width of the piping zone recorded from the bottom camera. It is noticed that the maximum depth of erosion occurs on the upstream side while the maximum bottom width of erosion occurs on the downstream

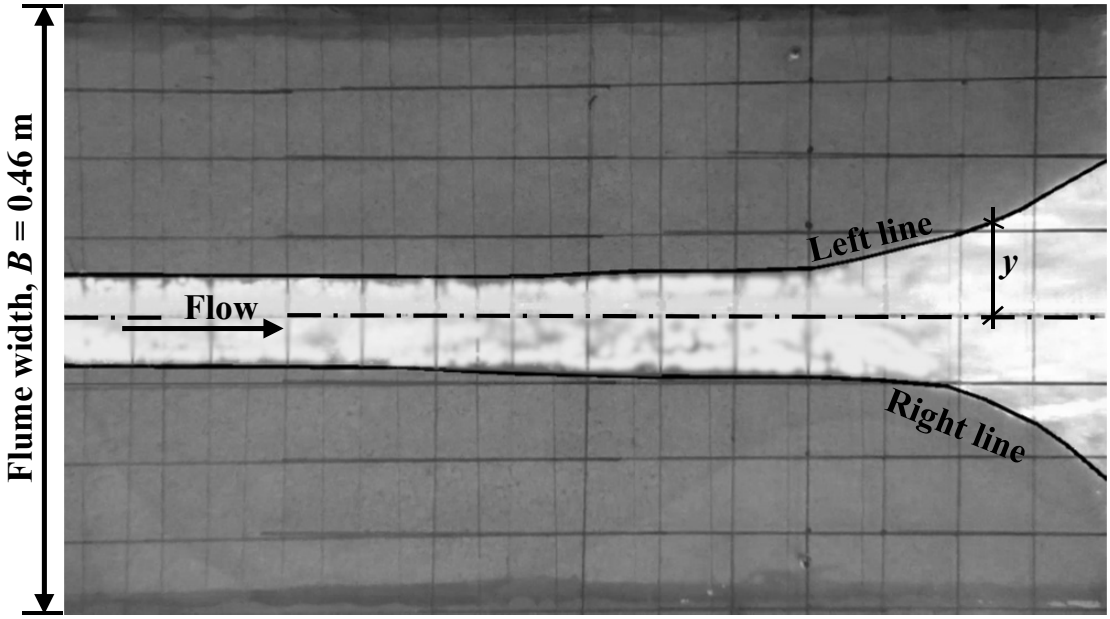

(b) View from bottom looking upwards.

Figure 4.2: *Continued*

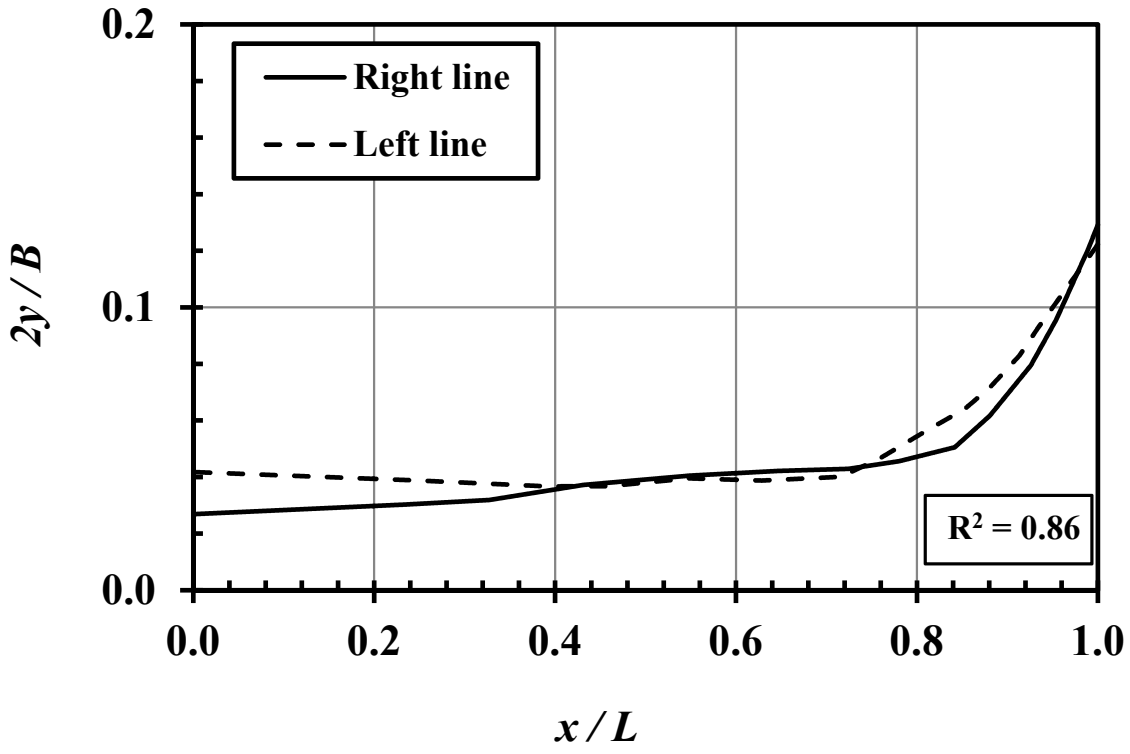

(c) Ratio of $2y/B$ for the bottom and top line.

Figure 4.2: *Continued*

side. This notwithstanding, the ratio of the average depth to the average width from all the experiments is found to have an average value equal to 0.98 ± 0.1.

The run time, t_f, for the case of n_b equal to 5, 10, 15, 25 and 35 are 20, 53, 140, 433 and 1241 s respectively, with an average standard deviation of 15%. From these results, the duration over which a relatively constant water surface elevation is maintained may be calculated using the relationship, $t_f = 13.4e^{0.135n_b}$ (R^2 of 0.98).

From the measured values of the average depth of erosion for different number of blows, best fit curves are obtained as an exponential function having the form

$$\frac{Z_{av}}{H_w} = \frac{d_{in}}{H_w} + 0.14n_b^{-0.81}e^{2.65\left(t/t_f\right)} \tag{4.1}$$

Curves are plotted in Fig. 5.2a for Z_{av} as function of $(n_b, t/t_f)$ with a step value $\Delta n_b = 5$. The plot shows that as the number of blows increases, the difference in the average depth, Z_{av} decreases. For this soil mixture, increasing the number of blows beyond 35 has insignificant effects on the average depth of erosion although the run time increases significantly. Figures 4.3b, 4.3c and 4.3d show comparison between measurements and estimates (Eq. (4.1)) along with the R-squared values for three cases. The results demonstrate that the evolution of piping erosion depth with time can be related to the number of blows used for compaction of a specific soil mixture.

The area of vertical erosion recorded from the side camera, A_s, is calculated by integrating the area between the top erosion line and the bottom line of the embankment at the bed level. This is done at different time intervals as the piping zone enlarges. Curves may be fitted to express A_s as a function of $(n_b, t/t_f)$, having the following form

$$\frac{A_s}{A_L} = \frac{A_{in}}{A_L} + 0.21n_b^{-0.72}e^{2.39\left(t/t_f\right)} \tag{4.2}$$

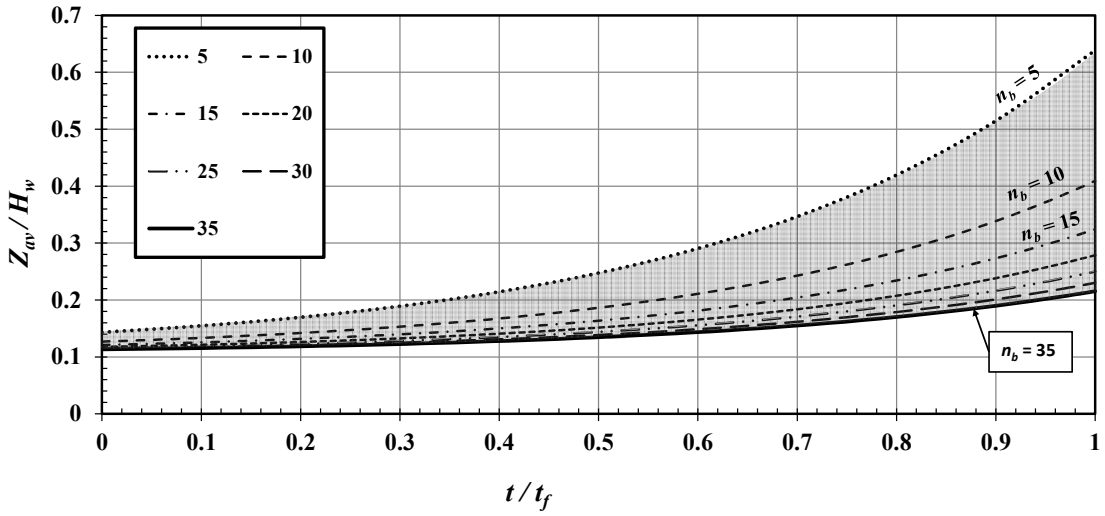

(a) Dimensionless Depth vs Dimensionless Time.

Figure 4.3: Empirical and experimental results for Z_{av}/H_w.

where, A_{in} is the initial side area calculated approximately as $d_{in} \times L$, in which L is the length of the embankment at the bed level, taken equal to 0.55 m in this study; A_L is the area of longitudinal-section of the embankment up to the water surface elevation. Figure 4.4a shows an envelope of curves for the fitted equation for A_s for different values of n_b. For the case of $n_b = 5$, more than 80% of the area has been eroded in an average time of 20 s as mentioned earlier. After this, the water depth decreases very rapidly from 0.11 m to 0.05 m in less than 8 s followed by a roof collapse. Figures 4.4b, 4.4c and 4.4d show the comparison between measurements and estimates from Eq. (4.2) along with R-squared values for three different values of n_b.

The change in the eroded volume of the piping zone with time is estimated from the recorded images using two approaches. In one, information from images taken by both bottom and side cameras are used. In the other, images from only the side camera are utilized.

Since a 3D view of the piping zone during the experimental run is not available, it

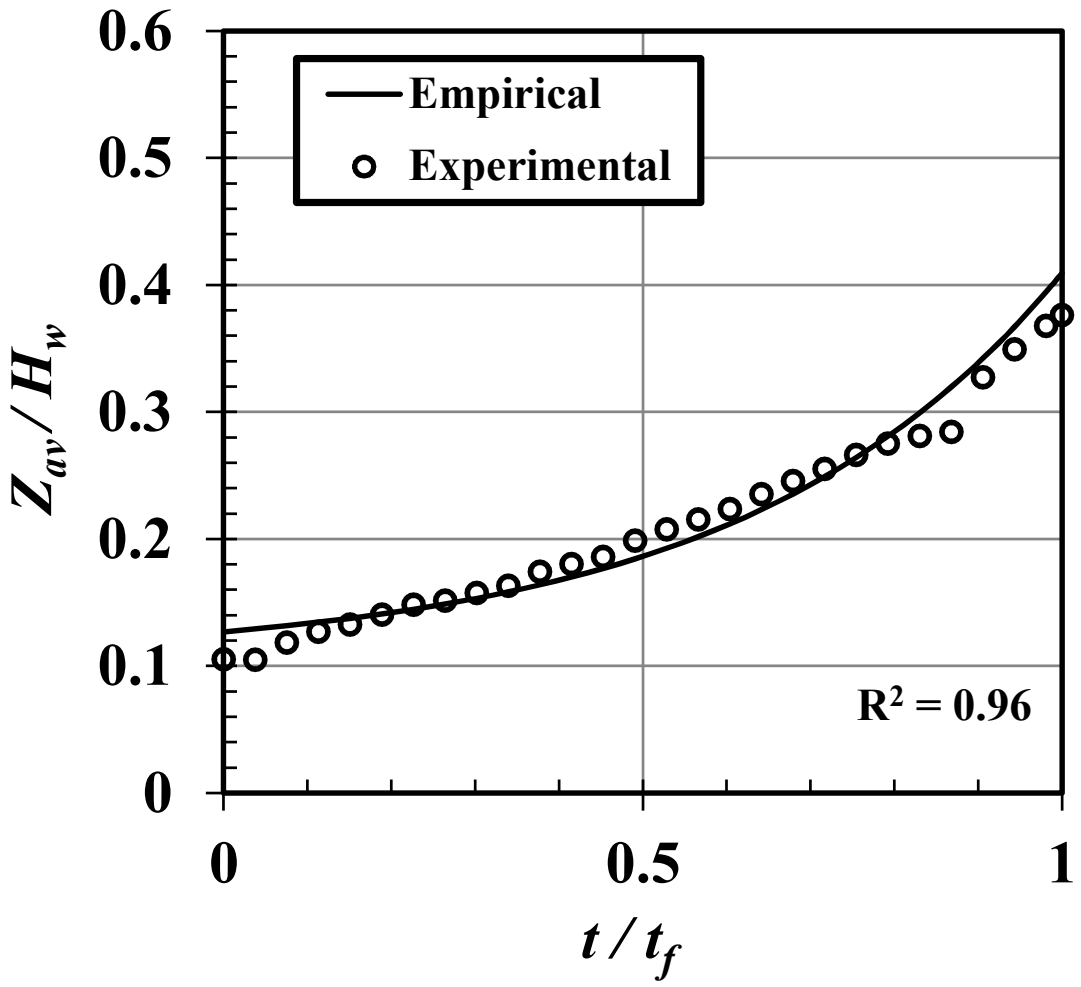

(b) $n_b = 10$

Figure 4.3: *Continued*

is assumed that the piping cross section maintains the same shape at a given location for the duration of the experiment. Eight different cross sections are cut along the embankment to delineate the final 3D shape of the piping zone after a run was completed. Figures 4.5a and 4.5b show the cross sectional shape of the piping zone at x = 300 mm and $x = 500$ mm, respectively from the upstream toe of the embankment. Figures 4.5c and 4.5d show the same cross sections after defining the edges. The shape of the top of the cross section may be approximated as quarter of a circle of radius y, equal to the width of the bottom erosion or radius Z, equal to the depth

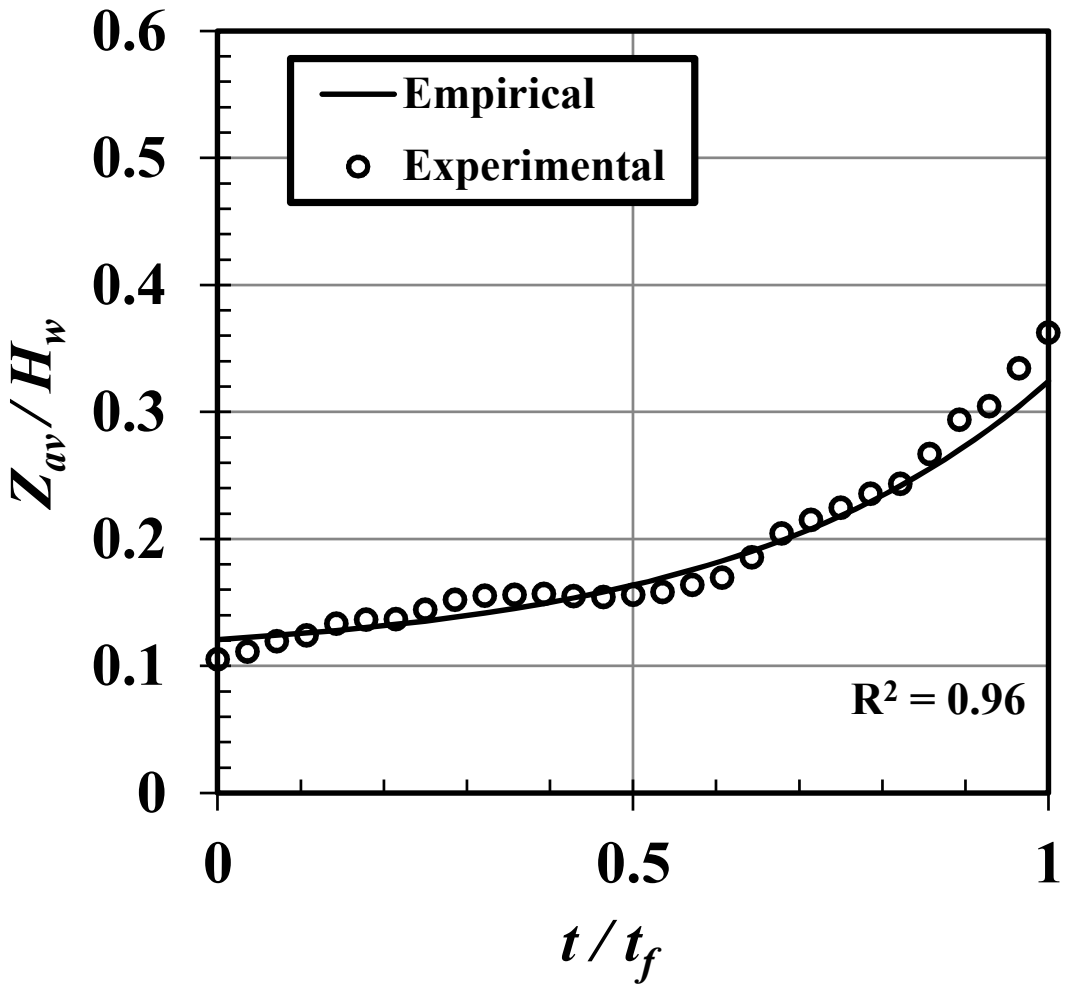

(c) $n_b = 15$

Figure 4.3: *Continued*

of erosion whichever is smaller. The bottom part is approximated as a rectangular shape with a variable height that depends on the depth of erosion relative to the width of erosion at this section, as shown in Figure 4.5e.

Since the depth and width of erosion is known at each section along the length of the embankment from the side and bottom cameras respectively, the first approach uses these data to integrate the approximated area of the cross section along the length to determine the volume. The second approach uses only the data from the

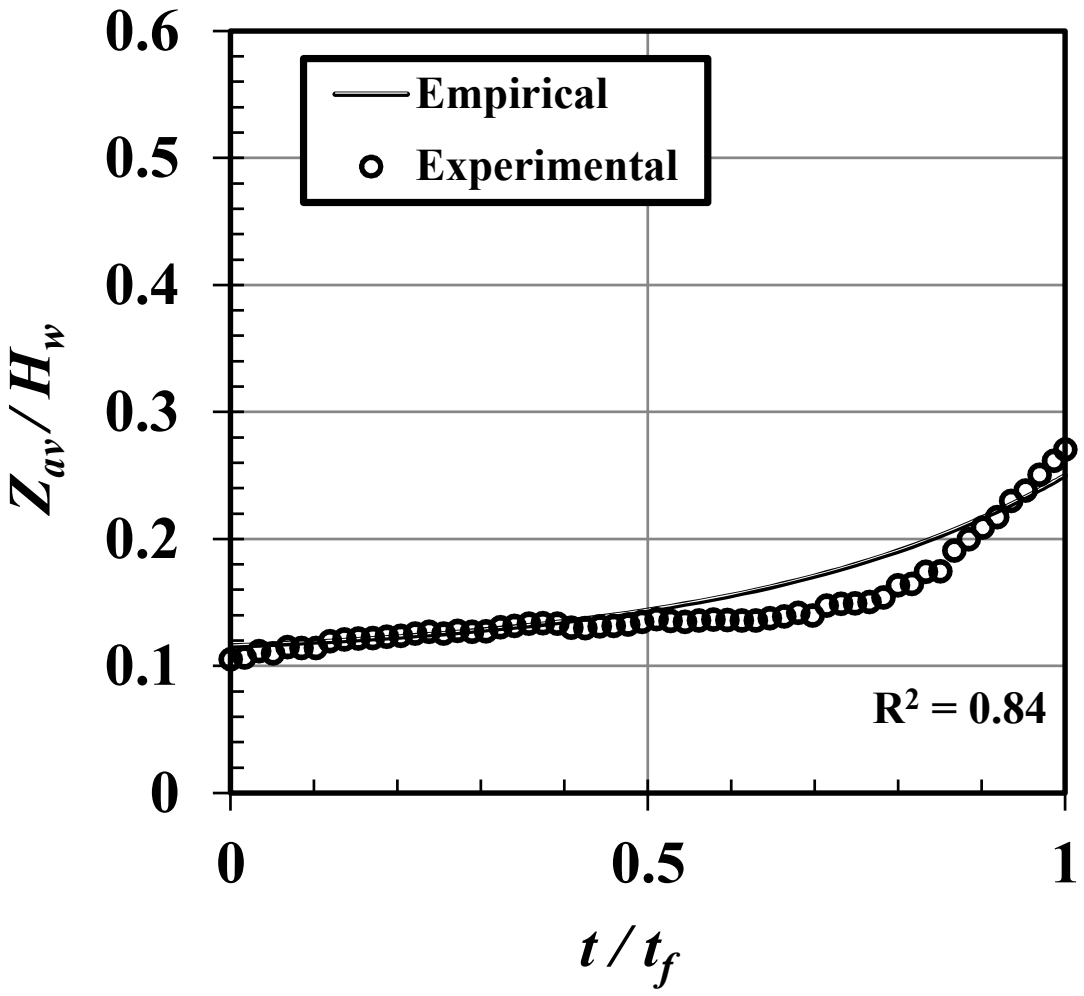

(d) $n_b = 25$

Figure 4.3: *Continued*

side camera, where the area of side erosion is multiplied by the average depth of erosion assuming that the average depth and width are approximately equal. The second approach is simpler than the first approach and it uses the data from only one camera to estimate the volume of the eroded material. Both approaches estimate the volume at different times.

By using the first approach, the experimental values for the eroded volume are

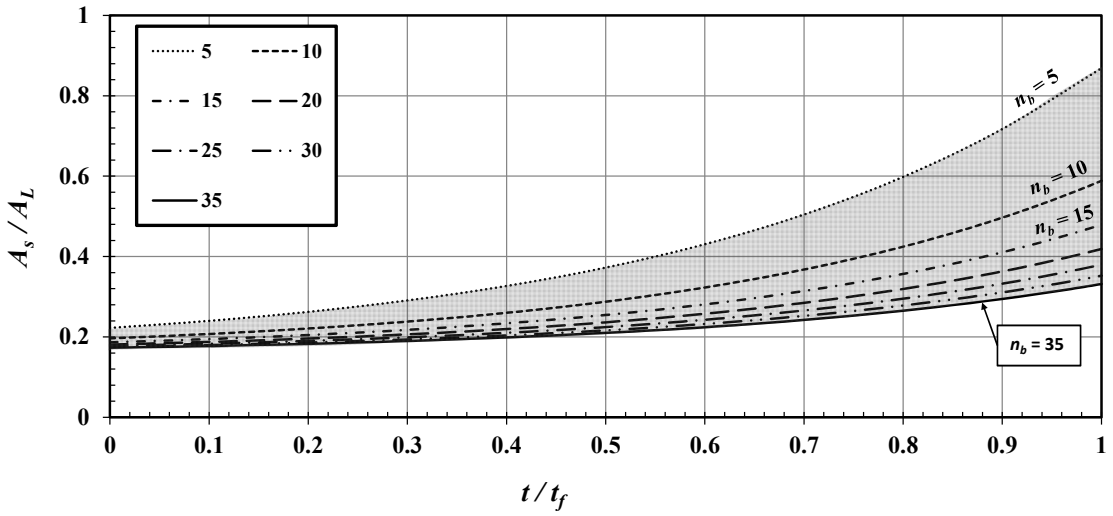

(a) Dimensionless Area vs Dimensionless Time.

Figure 4.4: Empirical and experimental results for A_s/A_L.

obtained and the results are fitted with the following empirical equation

$$\frac{V_1}{V_e} = \frac{V_{in}}{V_e} + 0.04 n_b^{-1.16} e^{2.75(t/t_f)} \tag{4.3}$$

where, V_1 is the calculated volume based on the first approach; V_{in} is the initial volume of the piping zone which is equal to $\pi/4 d_{in}^2 L$; V_e is the volume of the embankment up to the water surface elevation. Figure 4.6 shows the curves developed by applying Eq. (4.3) for different number of blows. The comparison between estimated values from experimental data and prediction by Eq. (4.3) gives R-squared values higher than 0.90 for all the experiments. As mentioned earlier, the eroded volume at the end of each experiment is measured, and this measured volume is superimposed on the curves, as shown in Figs. 4.6b, 4.6c and 4.6d. This demonstrates that the above methodology for estimating eroded volume with time provides a satisfactory agreement with the measured final volume of erosion.

For the second approach, the volume of the eroded material is calculated from the

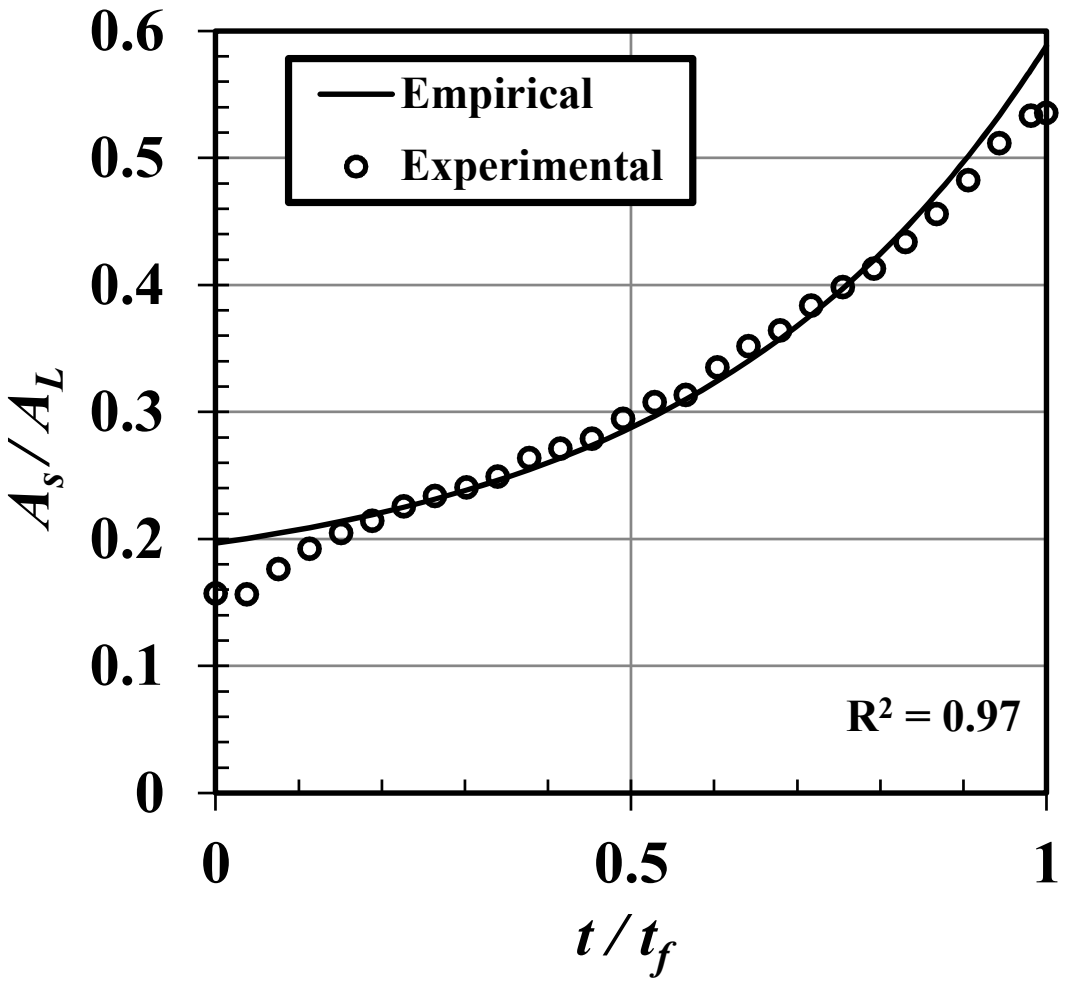

(b) $n_b = 10$

Figure 4.4: *Continued*

following fitted equation

$$\frac{V_2}{V_e} = \frac{V_{in}}{V_e} + 0.025 n_b^{-1.02} e^{3.19\left(t/t_f\right)} \tag{4.4}$$

where, V_2 is the volume calculated by using the second approach. This equation is compared to that of the first approach and it is found that the ratio of V_2/V_1 ranges from 1.03 to 1.19. The second approach is much easier to implement, but it overestimates the volume by about 20%.

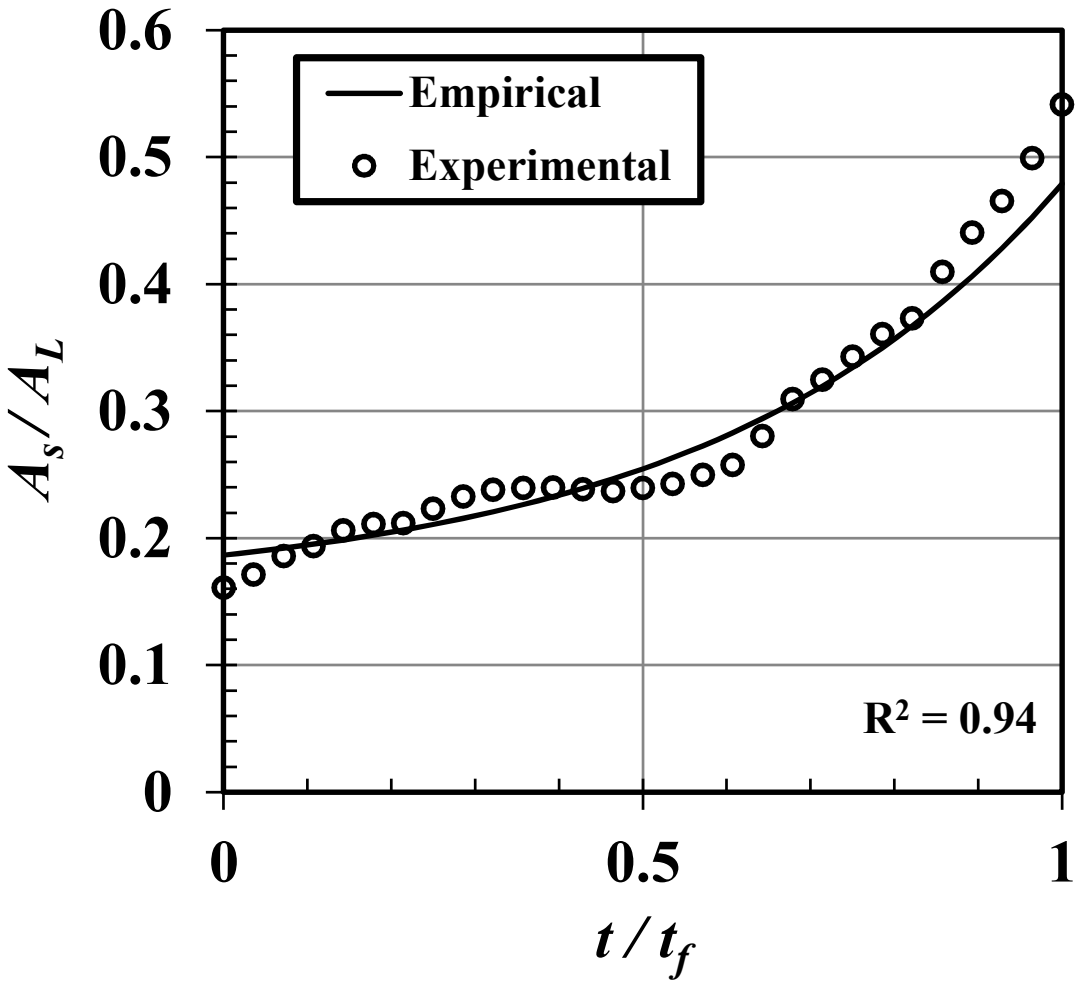

(c) $n_b = 15$

Figure 4.4: *Continued*

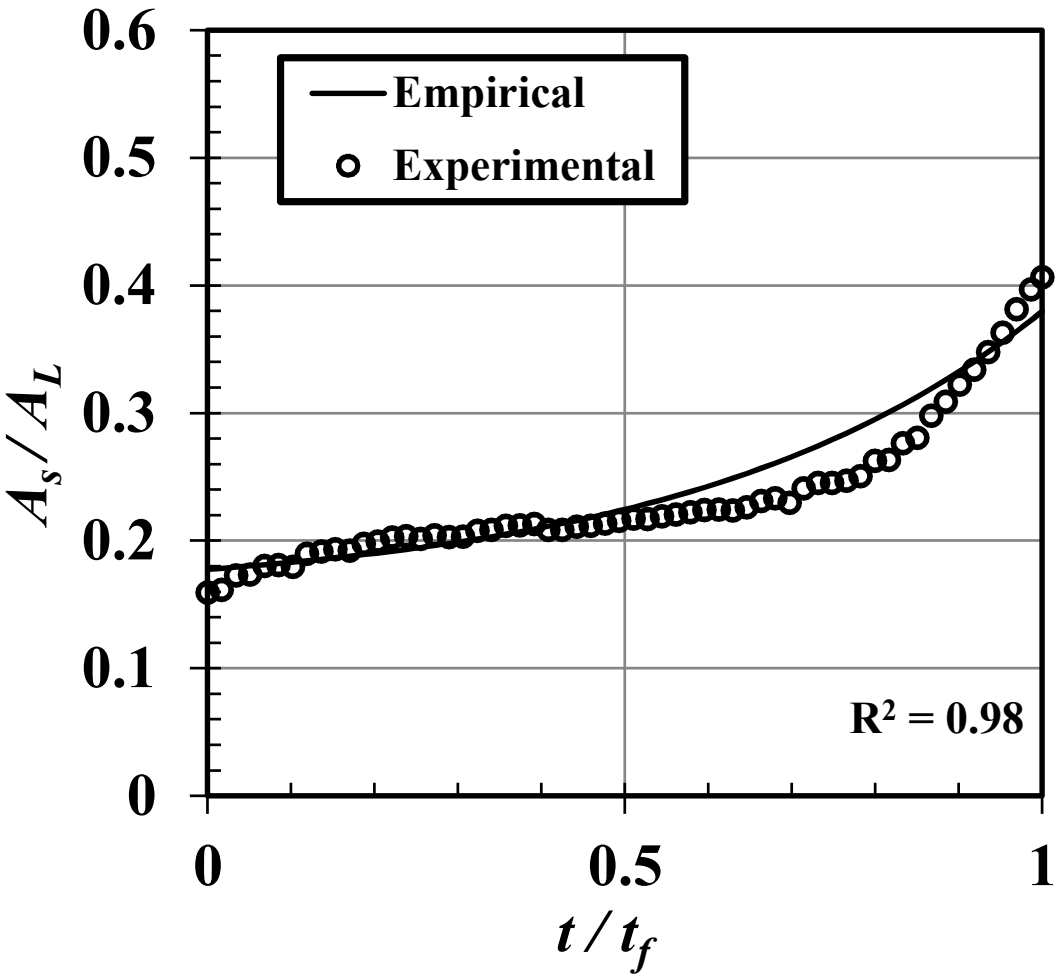

(d) $n_b = 25$

Figure 4.4: *Continued*

(a) Cross-section at $x = 300$ mm

(b) Cross-section at $x = 500$ mm

(c) After edge definition at $x = 300$ mm

(d) After edge definition at $x = 500$ mm

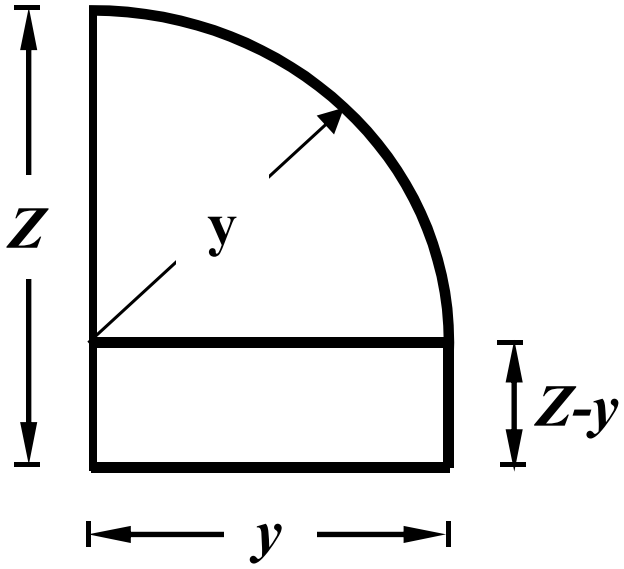

(e) Approximate shape of the cross-section

Figure 4.5: Approximate shape of the cross-section.

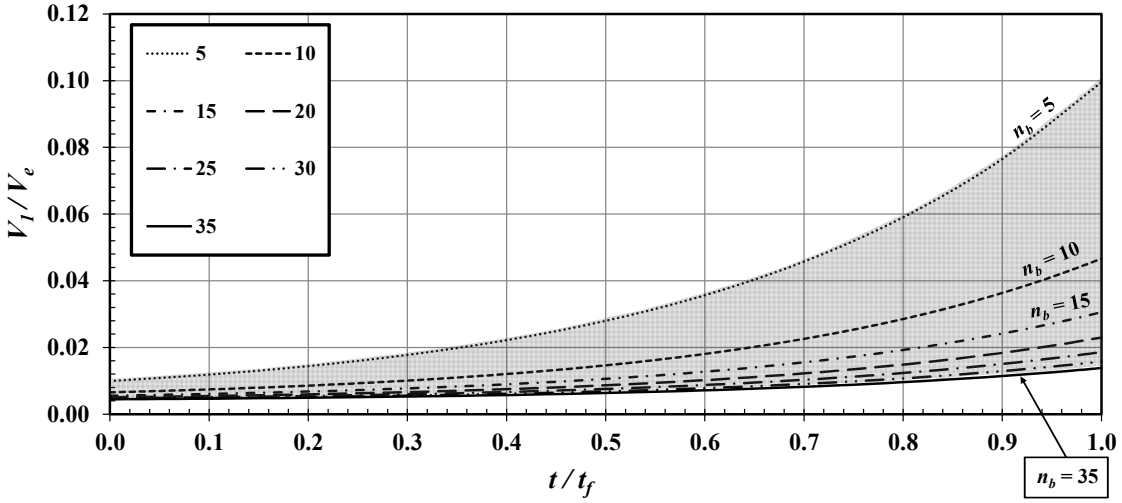

(a) Dimensionless Volume vs Dimensionless Time.

Figure 4.6: Empirical and experimental results for V_1/V_e.

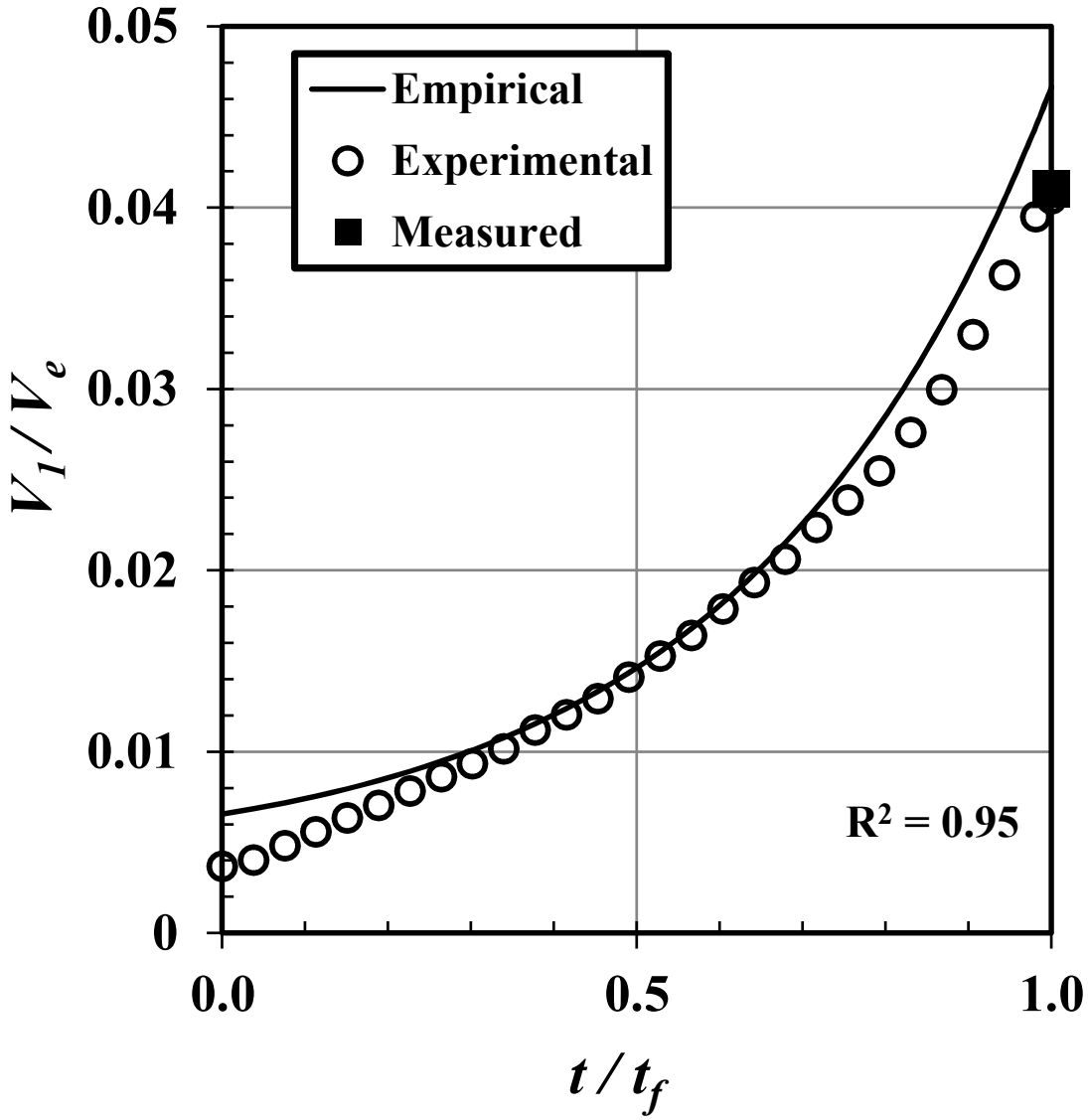

(b) $n_b = 10$

Figure 4.6: *Continued*

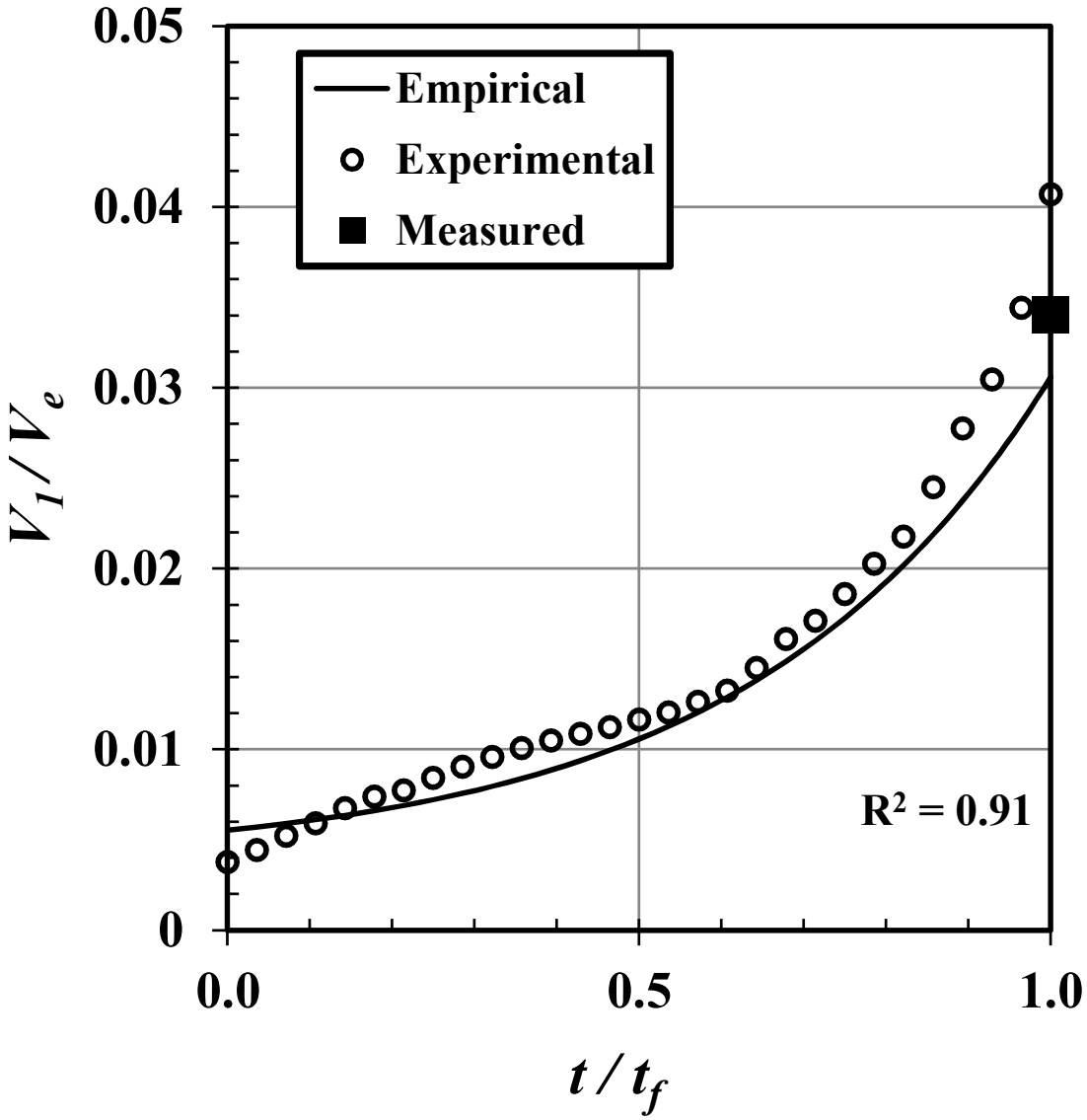

(c) $n_b = 15$

Figure 4.6: *Continued*

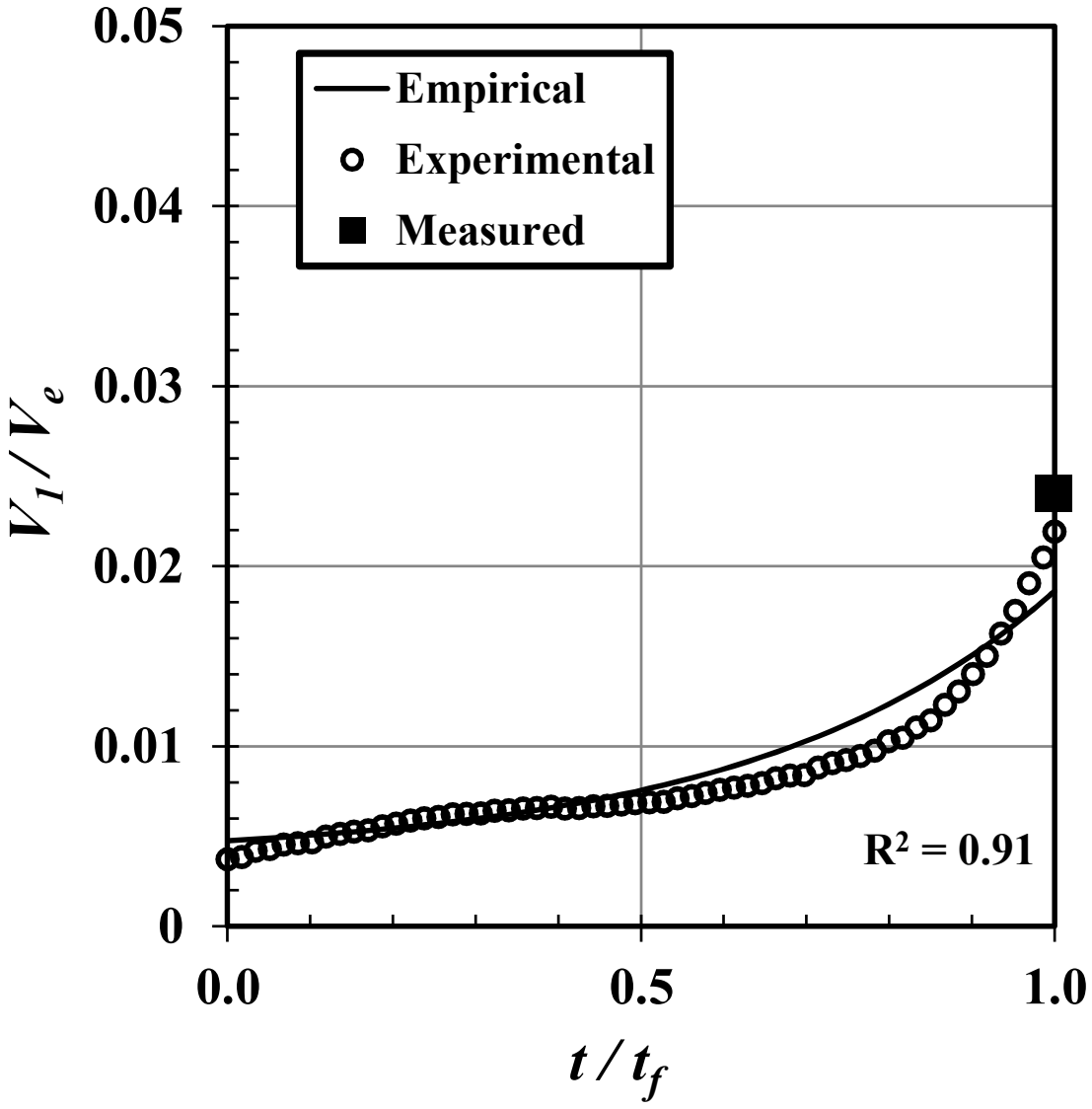

(d) $n_b = 25$

Figure 4.6: *Continued*

Chapter 5

Effect of Soil Mixtures

5.1 Introduction

At present there is no widely accepted method for the quantitative assessment of soil erosion resistance and potential erosion rates for clay-rich or "cohesive soils". This is due to the fact that it is difficult to determine accurately stresses caused by turbulent water flow on the soil surface and many of the factors that affect cohesive soil erodibility. The determination of the erodibility of clay-rich soil is important for assessing scour below or around hydraulic structures, stream-channel degradation, riverbank stability, soil losses from fields and the stability of embankments. Erodibility is mainly defined by two parameters: the critical shear stress which is created by the flow on the soil surface which initiates erosion and the erodibility coefficient which is defined by the ratio of the erosion rate of the soil to the excess shear stress on the bed. Many laboratory and in-situ techniques have been developed for use in laboratory and in-situ. These have included a rotating cylinder apparatus (Moore- and Masch 1962), a rotating annular flume (Krishnappan 1993), open-channel flume tests (Hanson 1990a), closed-channel tests, such as the Erosion Function Apparatus (Briaud et al. 2001), and the use of a vertical impinging jet in a number of different geometries with varying methods of analysis of the results (Bahsin et.al 1969; Hollick 1976; Hanson 1991; Tolhurst et al. 1999; Hanson and Cook 2004). A technique to determine in-situ erodibility is preferable for reliability. Because the soil is not disturbed by sampling, tests can be conducted using the in-situ water, as eroding water

chemistry is known to effect the soil erosion resistance (Arulanandan et al.1975).

For the in-situ measurements, an impinging-jet apparatus is mostly used. Out of different impinging jet-type techniques, Hanson and Cook (2004) method in ASTM Standard D5852 are increasingly being used to assess soil erodibility (Allen et al.1997; Shugar et al 2007, Thoman and Niezgoda 2008; Clark and Wynn 2007). This method presents time dependent anlytical procedures for using the jet test for quantitative estimation of both the critical shear stress and erodibility coefficient of a soil. But there are still some concerns about the reliability of a jet-type test for the assessment of soil erodibility (Annandale 2006). Therefore, a new approach that utilizes imaging technique has been adopted in this work to determine the erodibility coefficient and critical shear stress.

5.2 Methodology

The soil mixtures used in the experiment to study the erodibility coefficient of soil and critical shear stress during the piping failure are three different type of mixtures: the first mixture consists of 64% medium sand, 29% silt (sil-co-sil 106 manufactured US Silica) and 7% Kaolinite clay, the second mixture consists of 73% medium sand, 21% silt and 6% Kaolinite clay and the third mixture consists of 55% medium sand, 37% silt and 8% Kaolinite clay. The soil mixtures are changed for the experimental purposes but the number of blows is maintained constant in each experiment equal to 25 blows per each section in a layer.

5.3 Results

Figure 5.1 shows the bathymetry of the top erosion line every five seconds for different soil mixtures. From the figure, the maximum depth of erosion is for mixture 1 since it has the lowest percentage of clay content. Since the time interval of 5 s is constant,

Table 5.1: Soil properties

Soil properties	Mixture number		
	1	2	3
% Sand	73	64	55
% Silt	21	29	37
% Clay	6	7	8
porosity	0.38	0.36	0.4
c (kPA)	9.7	32.79	62.6
ϕ_{soil}	32	31.6	31.1
Water content %	9.5	9	8.6
$\gamma_{d\text{max}}$ kN/m^3	20.4	20.5	20.8

more erosion lines exist in the piping zone for the same drop of water from 0.13 m to 0.11 m for mixture 3 as compared to mixture 1. This means that increasing the percentage of clay from 6% to 8% significantly affects the run time of the experiment.

Similar plots are prepared for the change in the width of the piping zone recorded from the bottom camera. It is noticed that the maximum depth of erosion occurs near the upstream end while the maximum bottom width of erosion occurs near the downstream end. But, on an average scale, the ratio of the average depth to the average width from all the experiments is found to have an average value equal to 0.98 ± 0.1.

The run time, t_f, for mixture 1, 2 and 3 are 73, 433 and 1587 s respectively, with an average standard deviation of 22%.

From the results, trials are made to estimate the erosion coefficient, k_d from the rate of change of depth of erosion as well as the applied shear stress along the piping

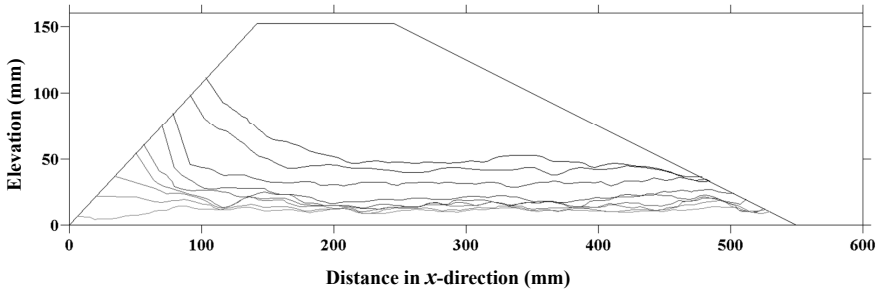

(a) Mixture 1

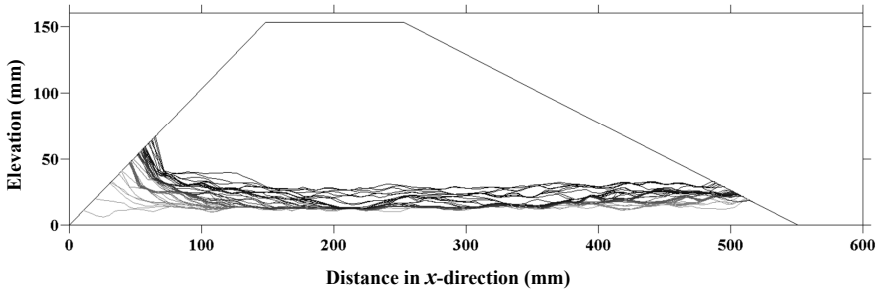

(b) Mixture 2

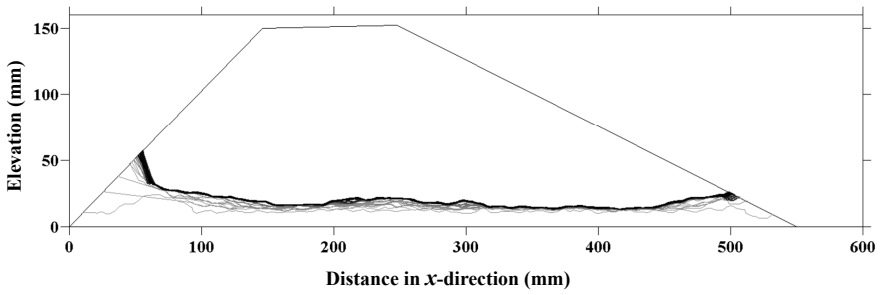

(c) Mixture 3

Figure 5.1: Bathymetry of the top erosion line every $t = 5$ s for different soil mixtures.

zone. The applied shear stress may be expressed as

$$\tau = \frac{\gamma \Delta h Z}{2L} \tag{5.1}$$

where Δh is the head loss along the piping zone and L is the length of the embankment at the axis of the piping zone and Δh, Z and L are all functions of time. From the analysis of the images, the depth of water at the exit of the piping zone may be assumed approximately equal to half the average erosion depth, Z_{av}. Thus Δh may be assumed equal to $H_w - Z_{av}/2$. The length of the embankment may be written as a function of the average erosion depth as $L = L_{base} - S_{us}Z_{av} - S_{ds}Z_{av}$, where, L_{base} is the length of the embankment at the bed level which is constant equal to 0.55 m; S_{us} and S_{ds} are the slopes of the upstream and downstream faces of the embankment equal to 1:1 and 2:1, respectively. The slopes are constant for the three soil mixtures tested.

From the measured values for the average depth of erosion for different soil mixtures, curves are best fitted as an exponential function having the form

$$Z_{av} = aH_w e^{b\left(\frac{t}{t_f}\right)} + d_{in} \tag{5.2}$$

in which, a is a constant equal to 0.0138 and b is a constant that depends on the coefficient of the soil erodibility, k_d and the total run time, t_f. Integrating the above equation and substituting it into Eq. (5.1), neglecting higher-order terms (O^2) and arranging the terms, the rate of change of the average depth of erosion may be obtained from

$$\frac{dZ}{dt} = \frac{2bL}{\gamma t_f \left(H_w - d_{in}\right)}\tau_b - \frac{bH_w d_{in}}{t_f \left(h_w - d_{in}\right)} \tag{5.3}$$

Erosion laws dealing with soil surface erosion by a tangential flow are often written as

$$\varepsilon = K_d \left(|\tau_b| - \tau_o\right) \quad \text{if} \quad |\tau_b| > \tau_o \tag{5.4}$$

where, ε is the erosion rate in volume per unit area per unit time; τ_b is the applied tangential shear stress at the interface and τ_o is the critical shear stress or the representative initial shear stress which is the minimum shear stress for initiation of erosion. From Eqs. (5.3) and (5.4), an expression for the coefficient of soil erodibility, k_d may be estimated. Substituting this expression for k_d into Eq. (5.2), the non-dimensional average depth of erosion may be estimated from

$$\frac{Z_{av}}{H_w} = 0.0138e^{\frac{k_d\gamma\,(H_w - d_{in})}{2L}t} + \frac{d_{in}}{H_w} \tag{5.5}$$

Analyzing the data for the three soil mixtures, the coefficient of soil erodibility, k_d in (m^3/t.s) are equal to 0.476 $\pm$ 0.185, 0.053 $\pm$ 0.016 and 0.014 $\pm$ 0.001 for mixture 1, 2 and 3, respectively. The corresponding erosion rate index, I, is equal to 1.0, 1.9 and 2.5 for the three mixtures, respectively. The duration over which a relatively constant water surface elevation is maintained may be calculated using the relationship, $t_f = 37.35k_d^{-0.86}$ with R-squared value equal to 0.99. It is worth to mention that the k_d value for mixture 2 is much less than k_d obtained from Hanson et al. (2010) for similar soil properties using the jet erosion test by almost 18.5%. On the other side, it agrees with that from the hole erosion test. This actually agrees with the concept that the dissipation of energy responsible for the erosion process and the nature of the hydraulic attack by the jet erosion test are completely different than that introduced by the flowing water in the flume. Also, it confirms the results (Wahl, 2010), that jet erosion test is not suitable for applications to internal erosion.

From Eq. (5.5), the curves are developed for Z_{av}/H_w as a function of $(k_d, t/t_f)$, as shown in Fig. 5.2a. It is clear that as the coefficient of soil erodibility increases, the average erosion depth, Z_{av} increases but with smaller rates. An increase in the k_d value from 0.01 to 0.05 m^3/t.s makes an increase in the average erosion depth by 22%, while an increase in the k_d value from 0.4 to 0.5 m^3/t.s makes an increase in

the average erosion depth by 6% only. Higher k_d values would not make much difference on the average erosion depth. Figures 5.2b, 5.2c and 5.2d compare the results from the measurements and values obtained from Eq. (5.5) along with the R-squared values. The results demonstrate that the previous equation may be used satisfactory to estimate the depth of erosion as function of both the coefficient of soil erodibility and time.

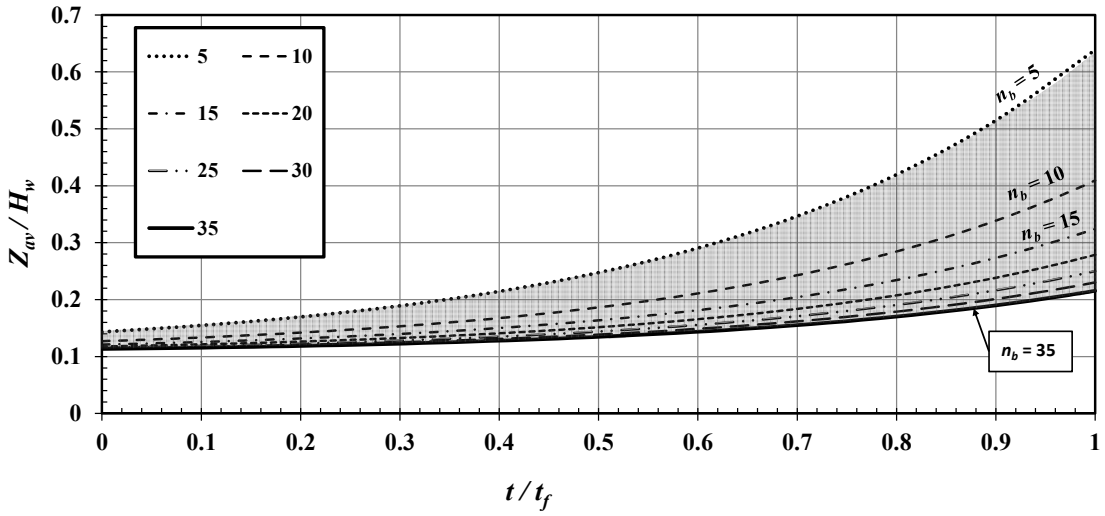

(a) Dimensionless Depth vs Dimensionless Time

Figure 5.2: Empirical and experimental results for Z_{av}/H_w.

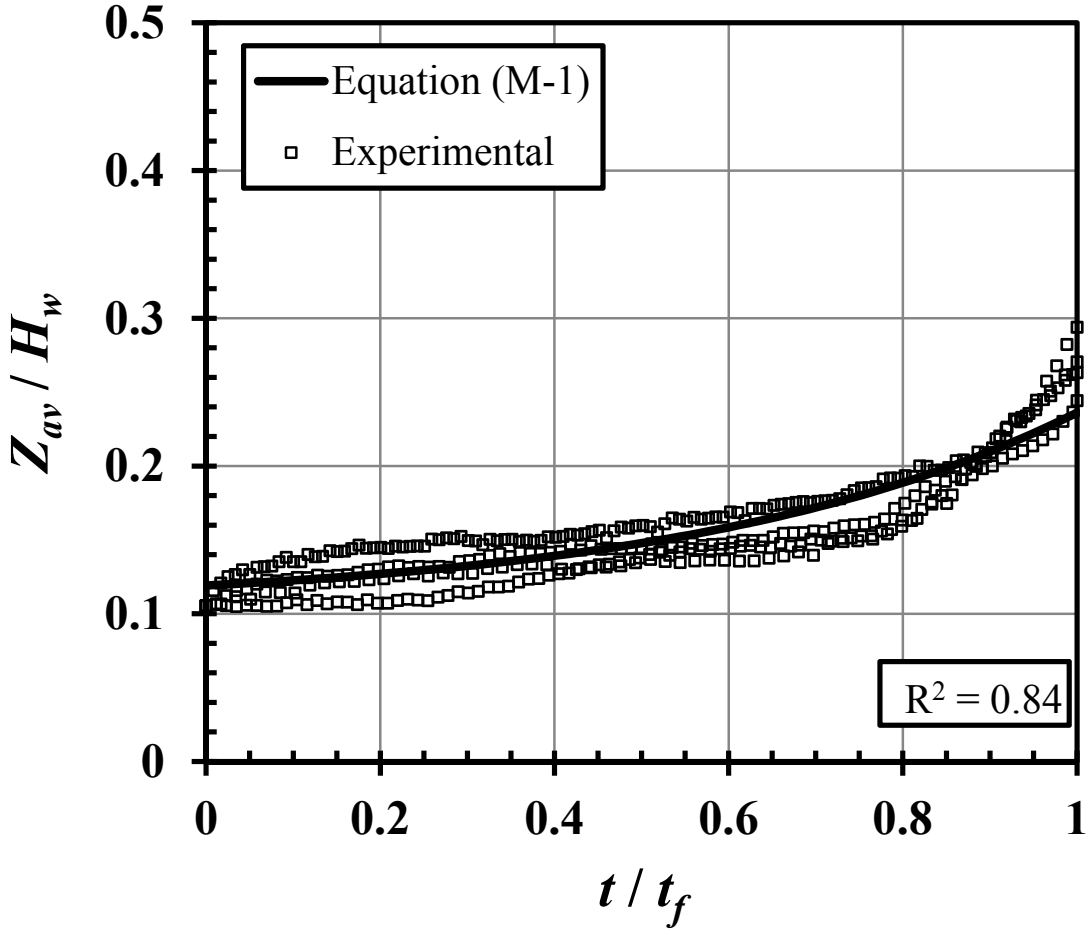

(b) Mixture 1

Figure 5.2: *Continued*

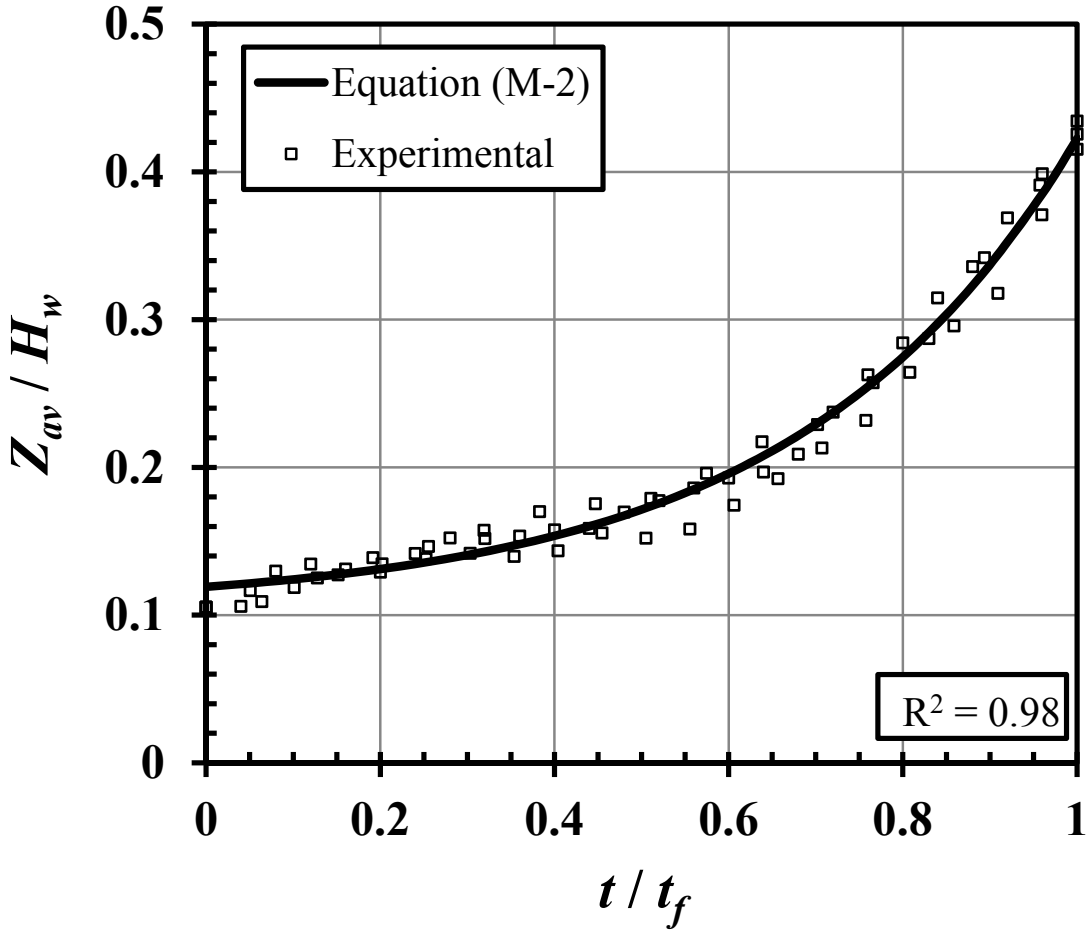

(c) Mixture 2

Figure 5.2: *Continued*

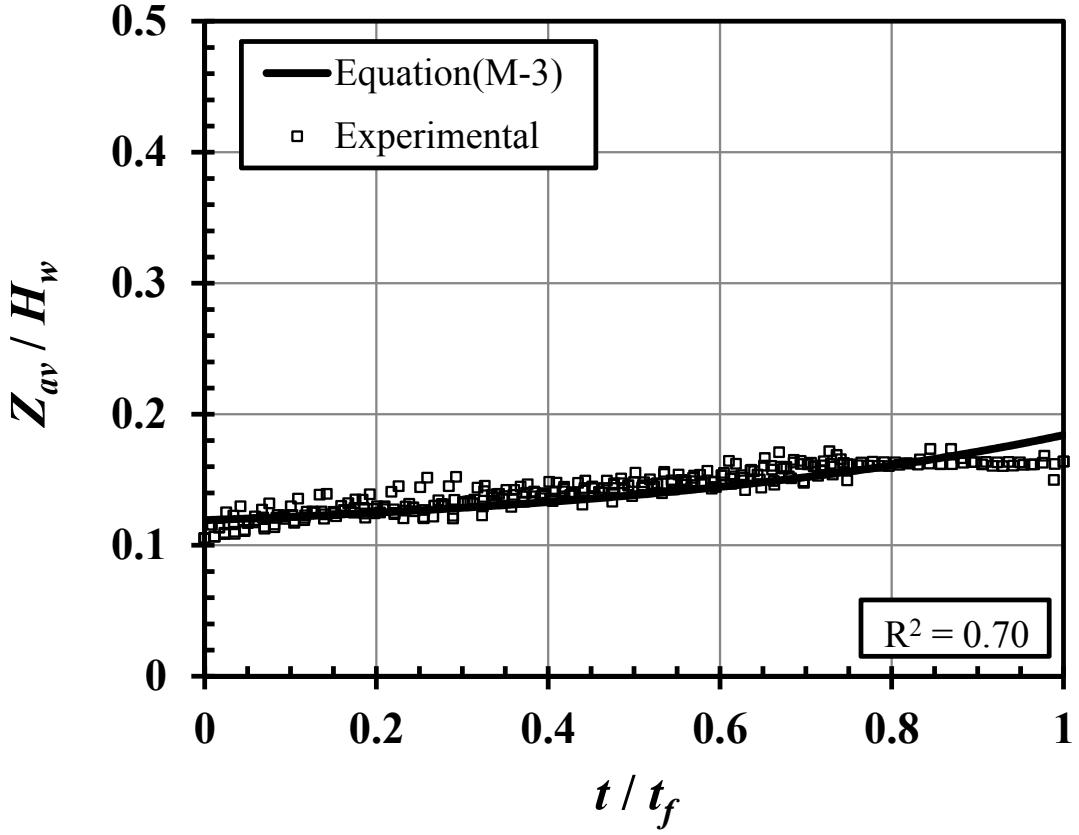

(d) Mixture 3

Figure 5.2: *Continued*

According to the values of the erosion-rate index introduced by Wan and Fell (2004b), the rate of erosion for mixture 1 and 2 is extremely rapid while that for mixture 3 is very rapid.

From the experimental results, the representative initial shear stress, τ_o may be obtained by extrapolating the results of ε versus τ to zero. It is found that τ_o has average values of 10.5 $\pm$ 0.9, 15.4 $\pm$ 1.7 and 15.6 $\pm$ 0.01 Pa for the three mixtures, respectively. These values are slightly higher than those obtained by Wan and Fell (2004b) for SM soil with fairly similar properties than mixtures used in this study. The maximum applied shear stresses at time, t_f are equal to 51.9, 41.2 and 23.7 Pa

for the three mixtures, respectively. The water velocity ranged from 0.9 m/s to 1.8 m/s based on an estimated value of k equal to 0.5 and f_b equal to 0.008, where, k is the head loss coefficient from section sharpening at the piping zone inlet and f_b is the turbulent friction factor.

Although the application of image processing technique for analyzing the internal erosion in a laboratory flume is difficult than applying the hole erosion test for estimating the coefficient of soil erodibility, it is more realistic as compared to the real-life applications. Care should be taken when extending these results to mixtures with different soil properties than those used in this study. Additional experiments with more soil mixtures and scales are needed to corroborate the applicability of the developed empirical relationship at the field scale.

Chapter 6

Numerical Investigation of Internal Erosion

6.1 Introduction

A large number of studies on the failures of embankments by overtopping have been conducted; however, in recent years studies on the failure by piping are limited. Sufficient reliable documentation on climate reservoir, topography, breach geometry, failure time, properties of embankment material (particle size, clay content, erodibility, construction method, cohesion and shear strength), etc. are needed to validate models for determining an embankment breach. Several procedures, both field and laboratory have been developed for characterizing the erodibility of earthen material including channel tests (Arulanandan and Perry, 1983), jet erosion test (Hanson, 1991; Hanson et al., 2010), slot tests (Wan and Fell, 2004a), rotating cylinders (Chapuis, 1986; Chapuis and Gatien, 1986) and hole erosion tests (Maranha das Neves, 1989; Reddi et al., 2000).

Real-life, full-scale field experiments are very important to understand complex natural phenomenon and validate embankment-breach models. Teton dam breach in 1976 is a well-documented piping failure real-life case study. A number of other real-life embankment failure cases have been reported (Balloffet and Scheffler, 1982).

Foster et al. (2000b,a) state that the internal erosion and piping have historically resulted in about 0.5% (1 in 200) embankment failure, and 1.5%(1 in 60) experi-

encing a piping incident. Failure by piping has not been studied as extensively as failure due to overtopping due to the difficulty in tracking the internal erosion process.

Experimental and field tests on internal erosion process have been reported by Hanson et al. (2010); Vaskinn et al. (2004); Awal et al. (2011) and van Beek et al. (2010). Lachouette et al. (2008) presented a one-dimensional model using diphasic flow volume equations and the jump equations to denote the fluid/solid interface to simulate the erosion process involved in the piping phenomena. They indicated that the particle concentration has significant effect at the beginning of the erosion process but may be neglected afterwards.

Zhou and Zhou (2010) presented a 3D piping model using distinct element method to simulate the pore fluid flow and solid particle transport during piping in a micro-scale level and simulation results were consistent with the experimental observations.

Alamdari et al.(2012) developed a one-dimensional numerical model based on the mass-conserving, finite-volume method to simulate piping phenomenon in a circular tunnel until the radius of piping reaches its critical value prior to roof collapse.

A numerical model is developed in this chapter to predict the evolution of the internal erosion process by piping in an earthen embankments and to study the effect of different parameters on the erosion process. These parameters include the initial diameter of the piping zone, the upstream and downstream slope, the crest width and the initial water depth upstream of the embankment. Different soil mixtures and compaction rates are used with a continuous flow and constant upstream head.

The run time in seconds, t_r, may be estimated from the following equation for the

number of blows, n_b and the coefficient of soil erodibility, k_d in the following form with r-squared value equal to 0.95

$$t_r = \frac{1.35}{k_d^{0.78}} e^{0.135 n_b} \tag{6.1}$$

DPTV (Digital Particle Tracking velocimetry) software detects the horizontal lines but ignores the vertical lines in the image. Fig. 6.1 shows the final bathymetry of the erosion line to the nearest $\pm$ 1 mm represented by the points with the highest magnitude across the width of the horizontal line. Missing points on the sides are extrapolated to the boundaries to have an erosion line that fully extends from the upstream edge to the downstream end.

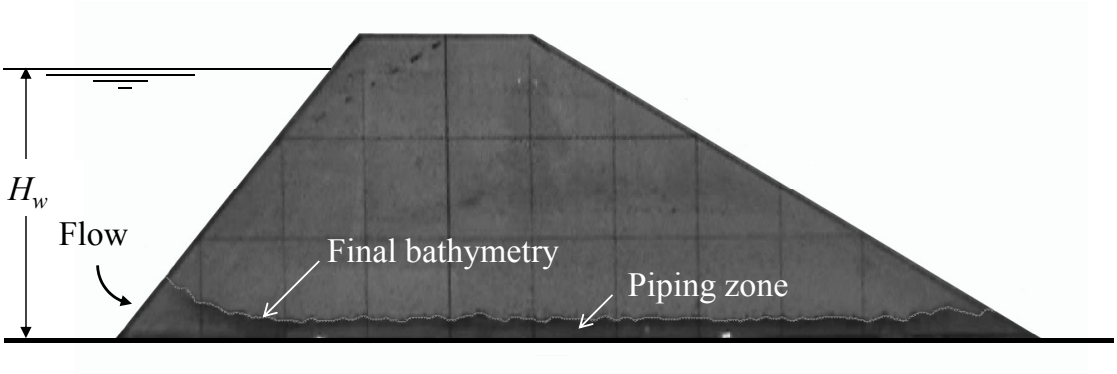

Figure 6.1: Final bathymetry of the erosion line from the image processing.

Figure 4.2a shows a comparison of four different runs for the case of $n_b = 25$ blows/section. In this figure, the x-axis represents the dimensionless time, t/t_r and the y-axis represents the dimensionless average depth of erosion in the piping zone, z/H_w, where t is the actual time in seconds; t_r is the run time, i.e., the time taken for the water surface elevation to drop from 0.13 to 0.11 m; z is the average depth of the piping zone and H_w is the initial upstream water depth which is equal to 0.13 m.

6.2 Numerical Model

A one-dimensional numerical model to predict the evolution of the internal erosion in an earthen embankment is developed. For 1-D approximation, the model is capturing only the change in the depth of erosion (vertical erosion), which means 1D process. The size of the initial piping configuration, the initial water level in the reservoir and the geotechnical characteristics are input to the numerical model. The model uses two modules: one for the pipe flow to estimate the rate of flow and the second for the boundary shear stress in the piping zone at a given time due to steady flow caused by the difference in head between the upstream and downstream end of the pipe. The friction factor, $f = 0.066$, is assumed constant based on measured experimental values. The rate of flow, Q is calculated from the pipe flow equation

$$Q^2 = \frac{(H_w - h_d)\,\pi^2 z^5 g}{4fL} \tag{6.2}$$

where H_w is the initial water depth upstream of the embankment which is assumed constant during the run and g is the acceleration due to gravity. The rest of the parameters vary with time, where h_d is the water depth downstream of the embankment, equal to one-half of the depth of erosion at the downstream side, as observed from the experimental results; z is the average depth of erosion along the entire piping length and L is the length of the pipe. The length of the eroded pipe may be expressed as a function of the average erosion depth as

$$L = L_{base} - S_{us}z - S_{ds}z \tag{6.3}$$

where L_{base} is the length of the embankment at the bed level; S_{us} and S_{ds} are the slopes of the upstream and downstream faces of the embankment, respectively. The shear stress may be estimated from the following equation

$$\tau = \rho f_b u^2 \tag{6.4}$$

in which ρ is the density of the water; f_b is the turbulent friction factor and u is the average cross-sectional flow velocity in the pipe.

The other module in the model is to simulate the internal erosion of the soil inside the pipe. The sediment transport equation used in this model relates to a flow condition known as ï£¡plane-bedï£¡ transport, i.e. transport in the absence of significant bedforms. From the images, it can be seen that as the sediment is detached from the body of the levee and goes into suspension, it will not settle on the flume bed as the velocity in the piping zone is high enough to transport it outside the zone. The term "bed load" can be changed here since it is different than what happens in open channel. Here the erosion is flipped, sediment is detaching from the levee and goes down and it will never roll or slide on the "top erosion line" which is not the case for open-channel. The transport equation has the same form as that for Meyer-Peter and Müller (1948) (MPM) relations taken as

$$q_b^* = \alpha(\tau^* - {\tau_c}^*)^n \tag{6.5}$$

where ${q_b}^* = q_b/\sqrt{Rgd_{50}}d_{50}$, in which q_b is the volume bedload transport rate per unit width; R is the submerged unit weight of the mixture; d_{50} is the mean diameter of the soil mixture; $\tau^* = \tau/(\rho R g d_{50})$; α is a constant that is a function of the compaction rates, n_b and the coefficient of soil erodibility, k_d and ${\tau_c}^*$ is the dimensionless critical shear stress for the soil mixture.

After the calculation of the bedload transport rate, q_b, Exner equation is used to calculate the depths of erosion in the entire length of the pipe as

$$(1-\lambda)\frac{\partial z}{\partial t} = -\frac{\partial q_b}{\partial x} \tag{6.6}$$

where λ is the porosity of the mixture.

Exner equation is solved by using the forward finite-difference method to update the depths of erosion along the pipe. The computations are repeated until the run time t_r, as estimated from Eq. (6.1).

From the analysis of the experimental results and fitting it to the numerical results, the constant α may be estimated from the following equation by using a nonlinear least square method, with r-squared value equal to 0.99,

$$\alpha = 80.39e^{-0.17n_b}k_d \tag{6.7}$$

6.3 Results

Figure 6.2 shows a comparison between the results of the experimental erosion lines obtained from the digital image processing technique and the corresponding results from the numerical model. The numerical model has the ability to simulate the depth of erosion along the piping zone. It is noticed from the experimental results that the maximum depth of erosion occurs on the upstream side while the maximum bottom width of erosion occurs on the downstream side.

As mentioned previously, different tests are run with different soil mixtures and different number of blows for each section. The comparison between the experimental results and the numerical ones for different number of blows is shown in Fig. 6.3. From the figure, the maximum depth of erosion is for the case of $n_b = 10$. The maximum depth of erosion is 0.37, 0.33 and 0.25 for n_b values of 10, 15 and 25, respectively.

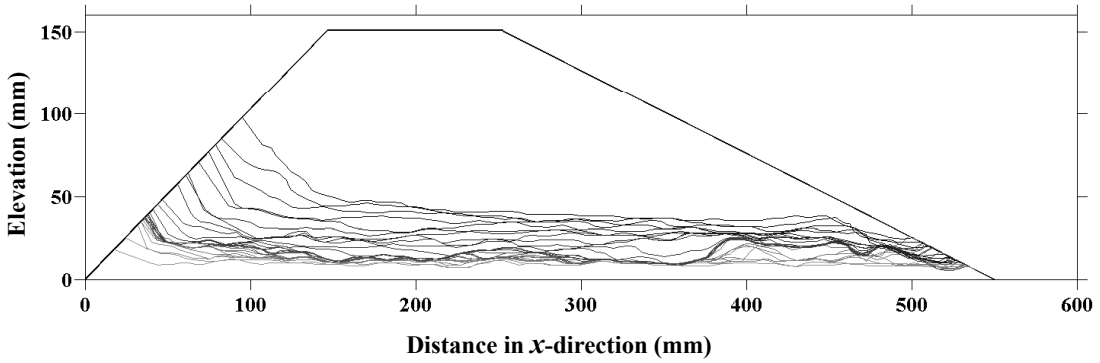

(a) Experimental result.

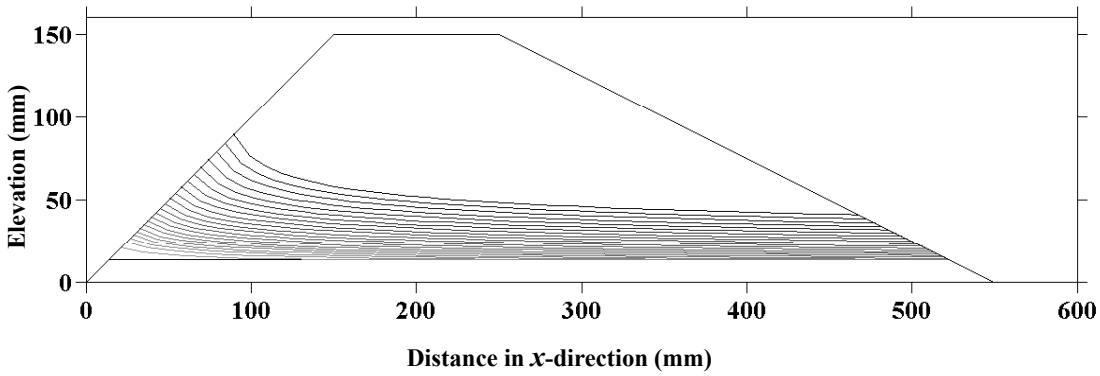

(b) Numerical result.

Figure 6.2: Comparison of experimental and numerical results.

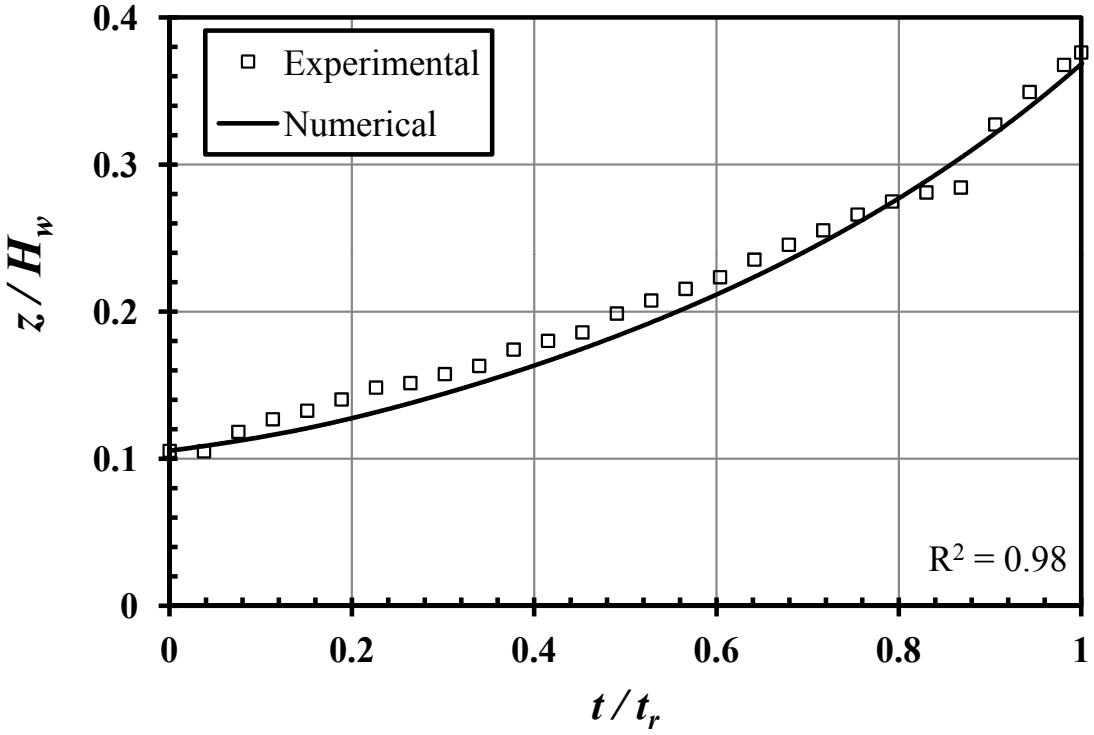

(a) $n_b = 10$

Figure 6.3: Comparison of experimental and numerical results for different n_b for mixture 2.

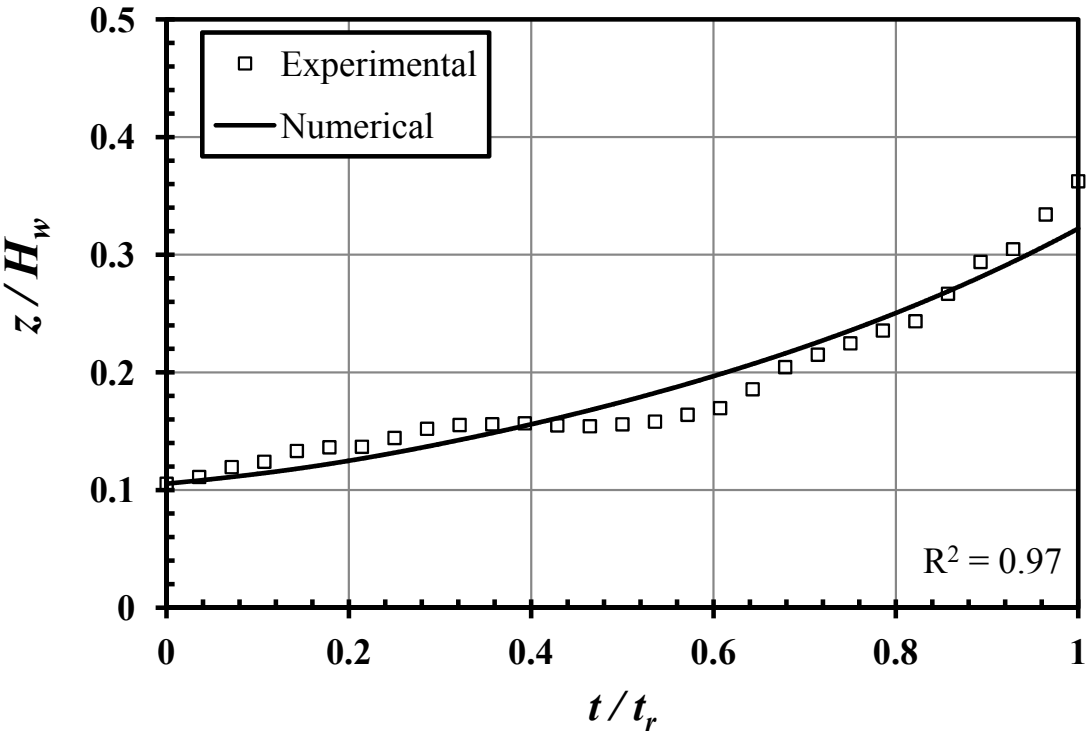

(b) $n_b = 15$

Figure 6.3: *Continued*

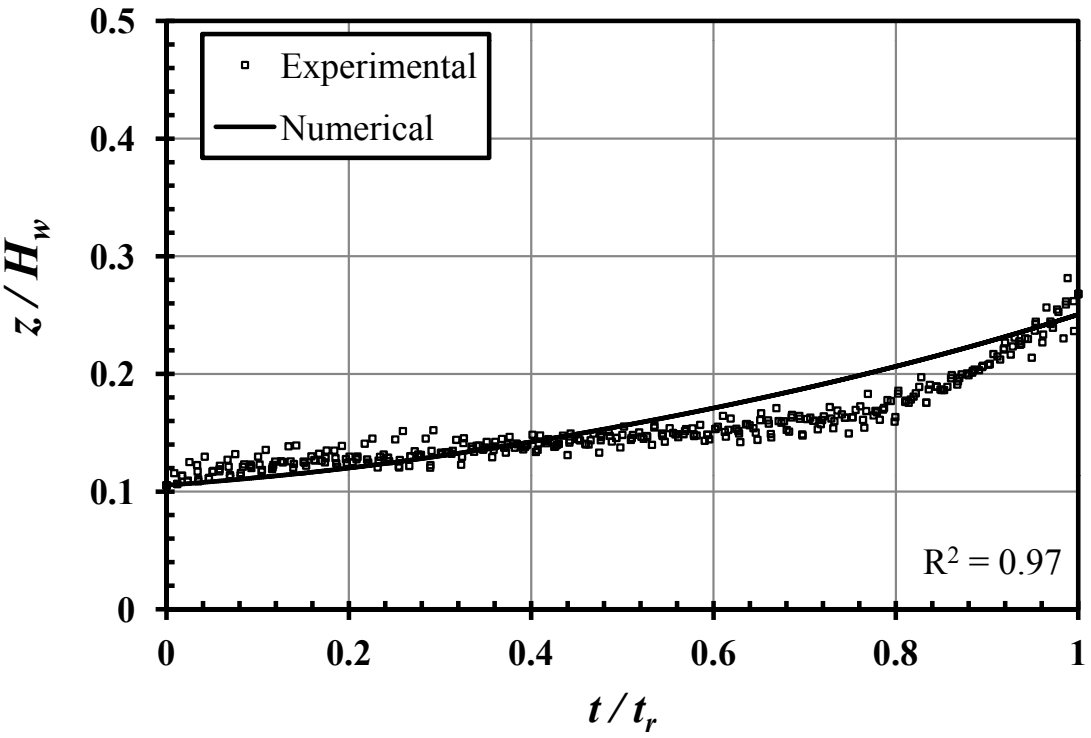

(c) $n_b = 25$

Figure 6.3: *Continued*

Similar plots are prepared for different soil mixtures. Figure 6.4 shows the comparison between the experimental and numerical results for the depth of erosion versus the time for different soil mixtures. As is clear from the figure, a change in the clay percentage significantly affects the depth of erosion. The depth of erosion in Mixture 1 is the least among the three mixtures tested since Mixture 1 has the least percentage of clay. The dimensionless depth of erosion is 0.41, 0.25 and 0.18 for Mixtures 1, 2 and 3, respectively. These results show that the numerical model may be used to determine the depth of erosion within the piping zone for different soil mixtures and compaction rates.

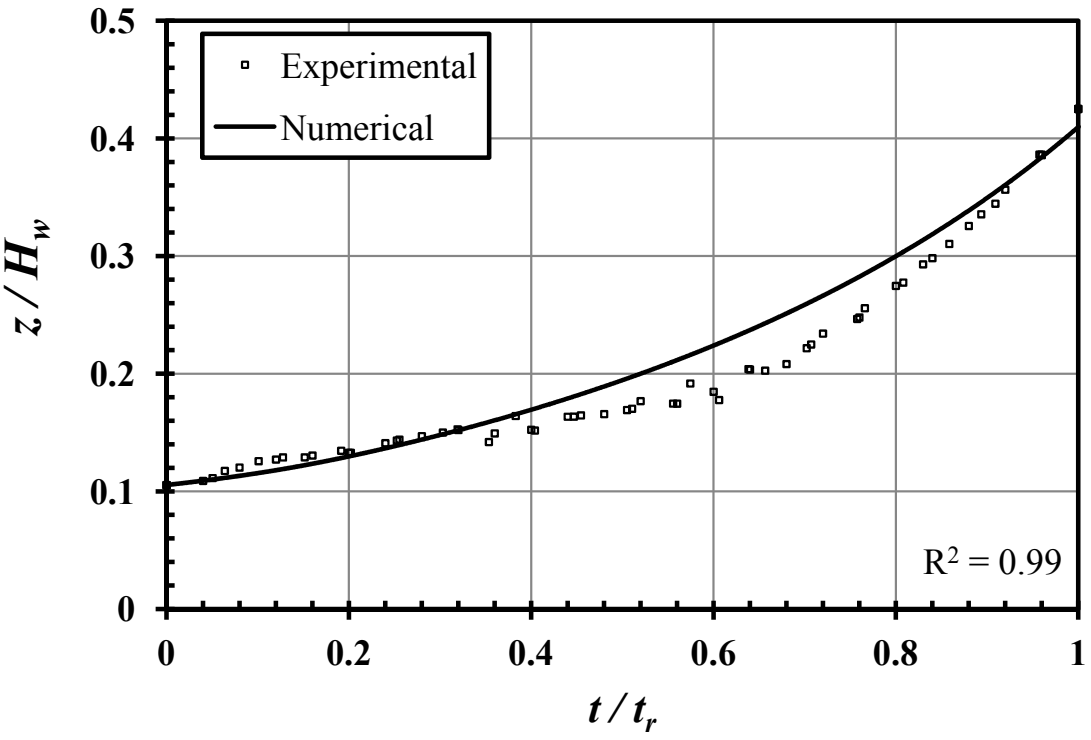

(a) Mixture - 1

Figure 6.4: Comparison of experimental and numerical results for different mixture.

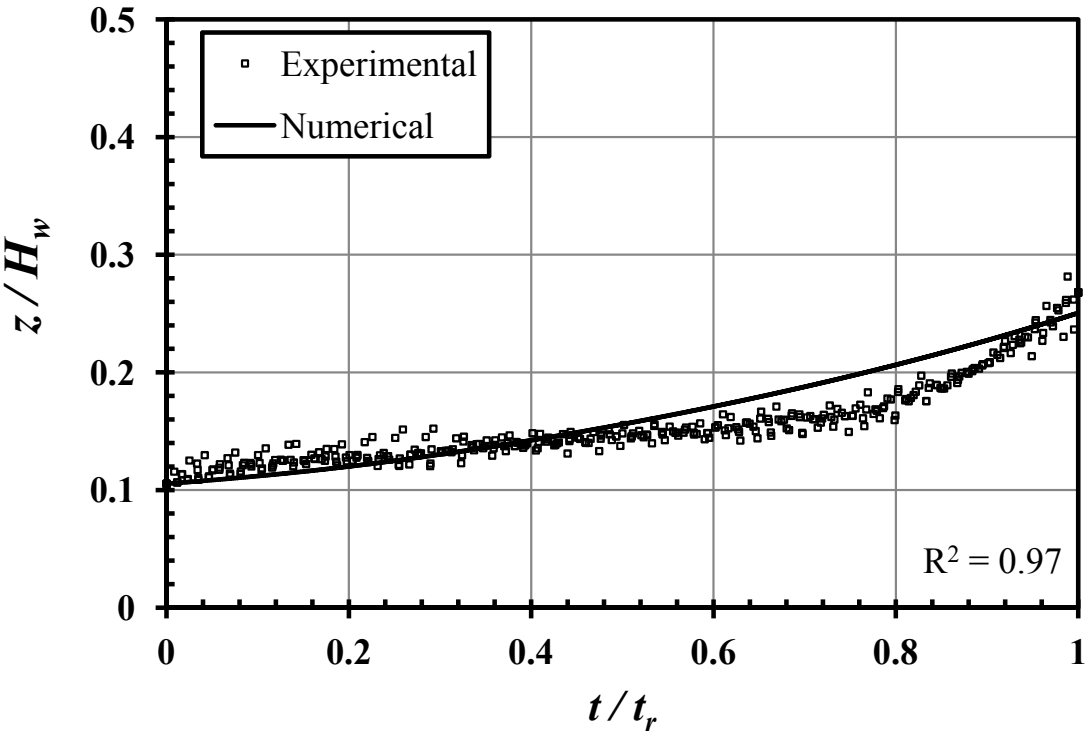

(b) Mixture - 2

Figure 6.4: *Continued*

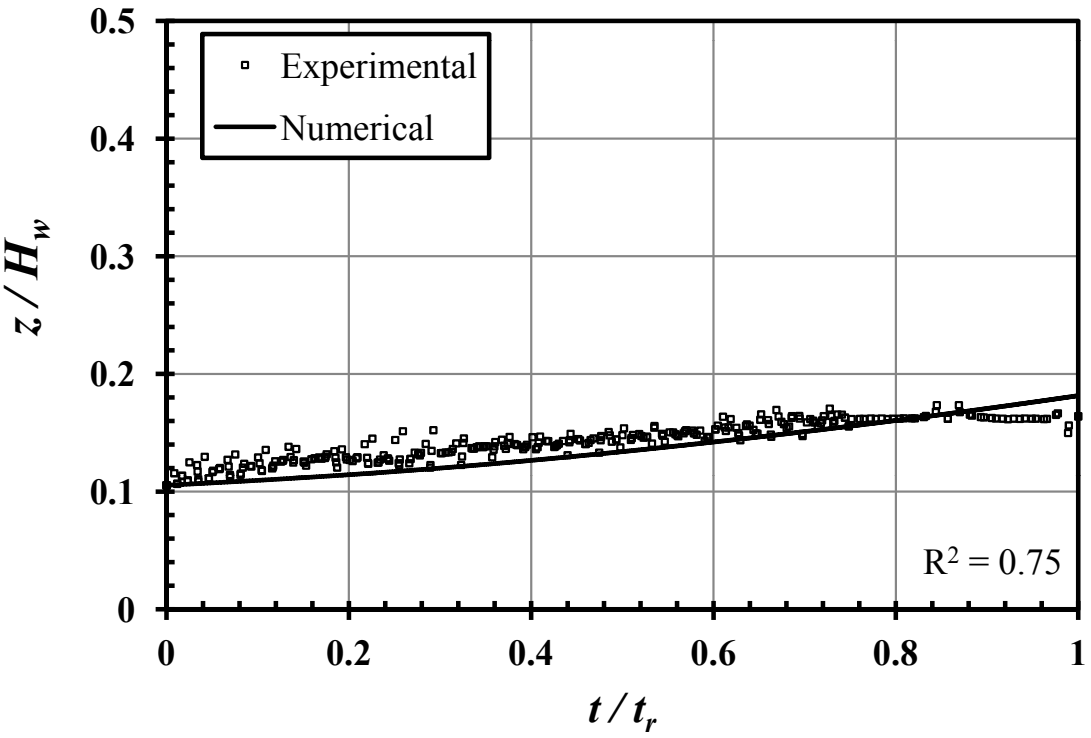

(c) Mixture - 3

Figure 6.4: *Continued*

Following parameters are analyzed to study their effects on the depth of erosion: the downstream and the upstream slope of the embankment, the crest width, the initial upstream water depth and the initial diameter. Figure 6.5 shows the effect of four different slopes on the average depth of erosion. In general, increasing the slope increases the depth of erosion. But, the effect of changing the upstream slope is higher than that of the downstream slope. A change in the upstream slope from 0 (vertical face) to 3 (i.e., 1:3) increases the depth of erosion by 33% while a corresponding change in the downstream slope, increases by only 16%.

The effects of other parameters on the average depth of erosion are shown in Fig. 6.6, keeping the upstream and downstream slopes as constant. Figure 6.6a shows the effect of increasing the dimensionless crest width, $C_r = L_c/L_b$ from 0% (i.e., trian-

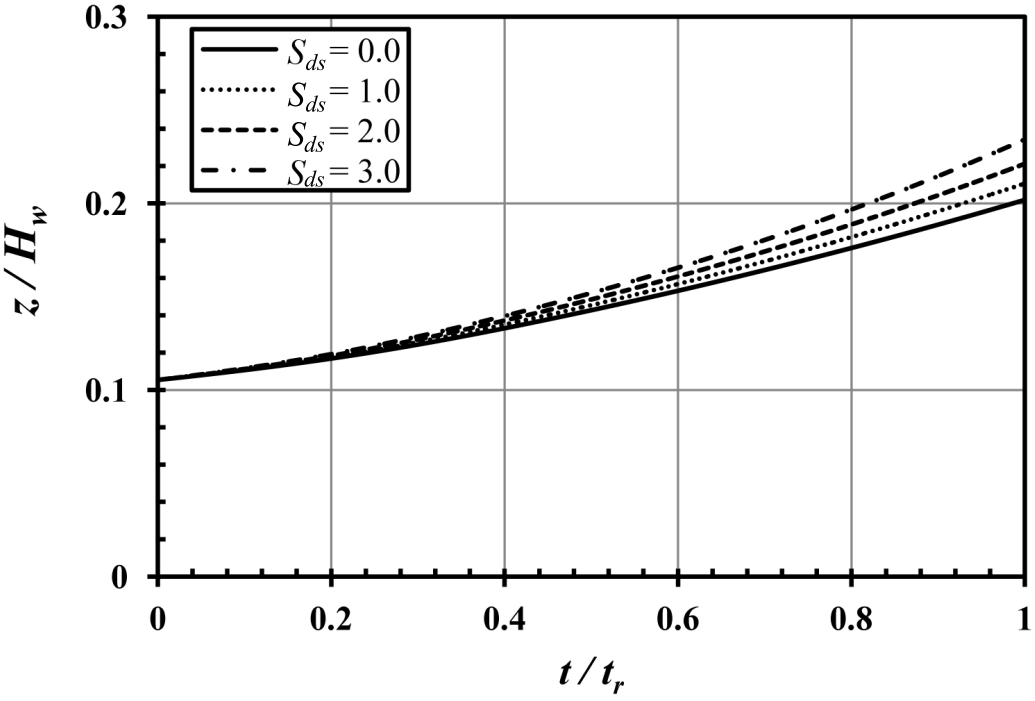

(a) Downstream slope

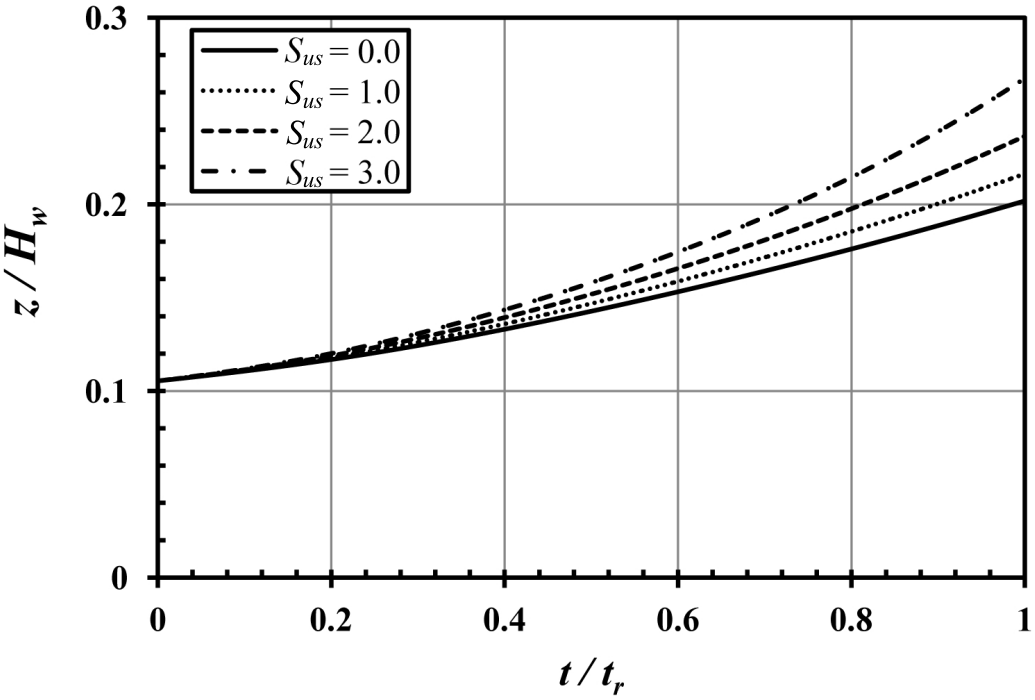

(b) Upstream slope

Figure 6.5: Effect of downstream and upstream slopes.

gle shape embankment) to 100% (i.e., rectangular shape embankment), in which, L_c is the actual crest width and L_b is the base length of the embankment. Increasing the crest width from $0 \sim 100\%$ causes a decrease in the average depth of erosion by 12%. In Fig. 6.6b, the effect of the dimensionless initial upstream water depth, $h_r = H_w/H_{dam}$ is shown, in which, H_{dam} is the height of the dam. A change in hr from $20 \sim 100\%$ causes an increase in the depth of erosion from its initial values from 7% to 54%. Finally, the effect of the dimensionless initial diameter, $d_r = d_{in}/H_w$, is presented in Fig. 6.6c. A change in d_r from $0 \sim 8\%$ has almost an equal effects on the change of the depth of erosion from its initial values and may be neglected. As expected, this analysis shows that the upstream water depth has the major effect on changing the depth of erosion since it plays an important role in governing the difference in head on the piping zone.

This study shows that a simple numerical model may be used to analyze piping phenomena in earthen embankment. However, testing of more soil mixtures and embankments at full scale are needed to verify the scale effect on the internal erosion process.

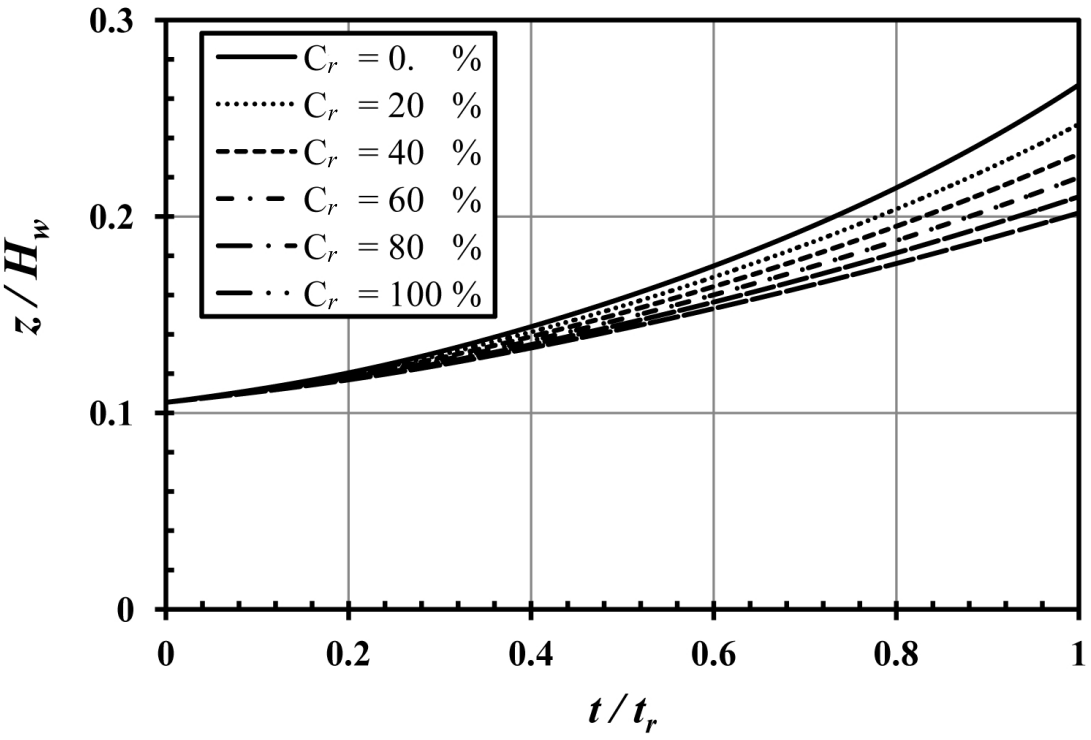

(a) Effect of crest width

Figure 6.6: Effect of crest width, initial water depth and piping diameter.

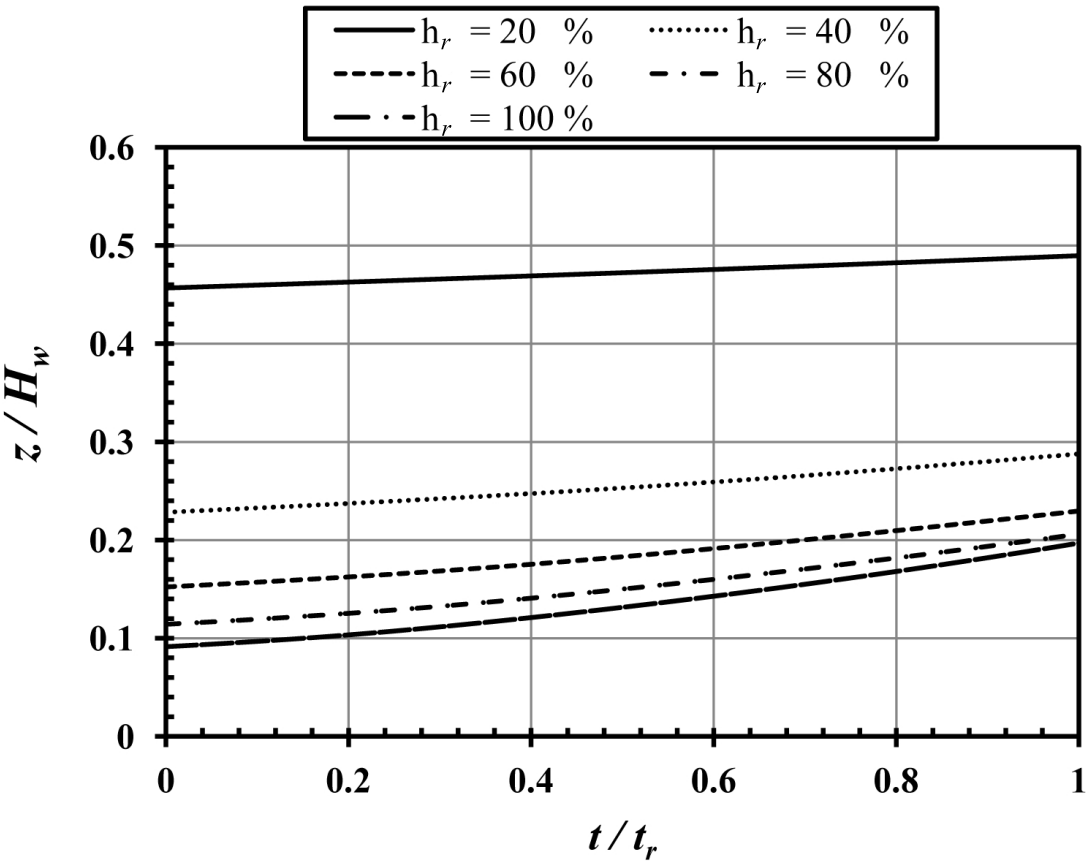

(b) Effect of initial upstream water depth

Figure 6.6: *Continued*

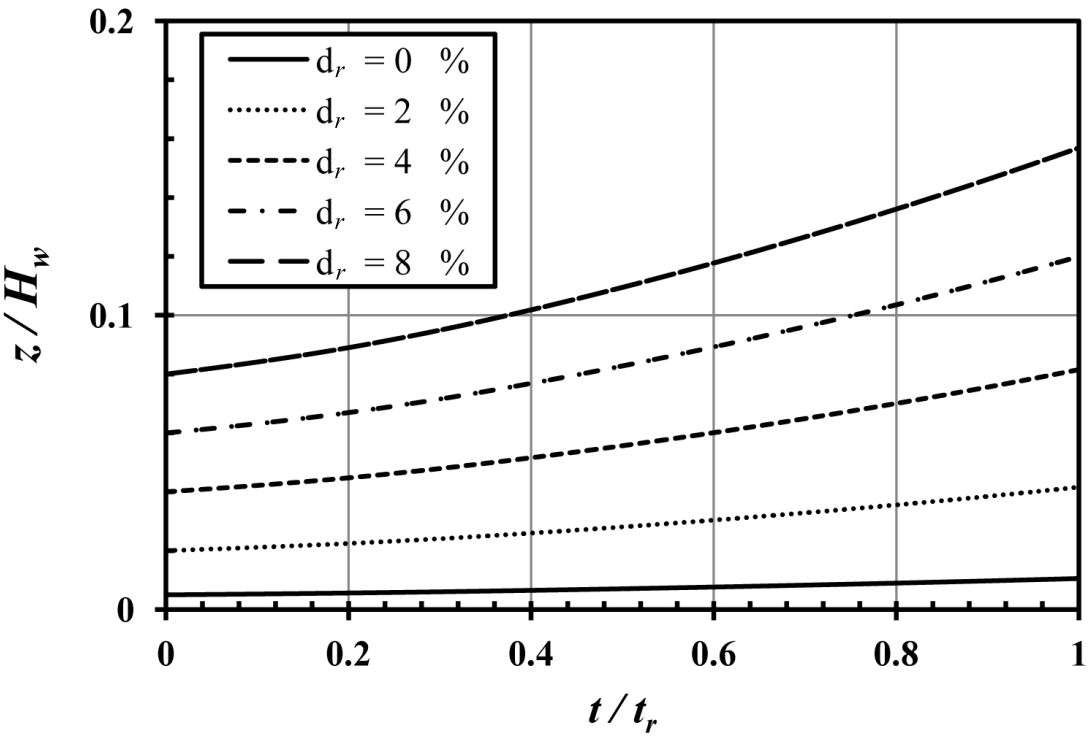

(c) Effect of initial piping diameter

Figure 6.6: *Continued*

The results show that increasing the compaction of the mixture per layer or the percentage of clay in the mixture decreases the average depth of erosion, with higher impact on the erosion rate from the clay percentage. The maximum depth of erosion occurs on the upstream side while the maximum bottom width of erosion occurs on the downstream side.

The effect of changing the upstream slope on the depth of erosion is higher than that of changing the downstream slope. In general, increasing the slope and the initial upstream water depth causes an increase in the erosion depth. Increasing the crest width causes a decrease in the erosion depth. The change in the initial piping diameter has a negligible effect and may be neglected.

Chapter 7

Summary, Conclusions and Recommendations

7.1 Summary

The results of this study shows that the compaction rate and soil properties significantly affect the erosion process in earthen levees. The maximum depth of erosion occurs on the upstream side while the maximum bottom width of erosion occurs on the downstream side. The ratio of the average depth to width is about one.

The experimental investigations provide a detailed description of the piping erosion process taking place in an earthen levee of a soil mixture. The measurement techniques and the methodology are described. The mixture is considered as sandy loam soil and is composed of sand, silt and clay with percentages of 64%, 29% and 7% respectively. Non-dimensional equations are developed to describe depth, area, and volume of erosion as function of time. Repeatability and symmetry of the experiment have been checked.

For the second experimental study, results show that the soil properties significantly affects the time of erosion to cause significant drop of reservoir level. Empirical equation is best fitted to the experimental results to estimate the depth of erosion as a function of time and the coefficient of soil erodibility. As the coefficient of soil erodibility increases, the average erosion depth increases but with smaller rates.

The development and verification of the numerical model by comparing the computed and measured results show promising outcomes. The numerical model may be used to study the effect and predict for different parameters on the piping failure of a levee.

7.2 Conclusions

From the results of the experimental investigations of compaction effect, the following conclusions may be drawn:

- Increasing the compaction of the mixture per layer, significantly affects the time of erosion to cause significant drop of reservoir level, however, it has a little effect on the average depth of erosion.
- The maximum depth of erosion occurs on the upstream side while the maximum bottom width of erosion occurs on the downstream side.
- The ratio of the average depth to width is about one.
- Two approaches are proposed for the estimation of the eroded volume. The first approach uses data from both side and bottom camera to estimate the volume while the second approach utilizes only the data from the side area. The second approach is much simpler but it overestimates the eroded volume as compared to the first approach.

For the results of the soil composition study the following conclusions may be drawn:

- The results for the coefficient of soil erodibility and the representative initial shear stress agree with that obtained from the hole erosion tests.
- The Jet erosion test is unsuitable to analyze internal erosion process.

- The image processing techniques may be applied for analysis of the piping erosion in earthen embankments.
- The proposed equation to estimate the depth of erosion may be satisfactorily applied for this type of soil.
- The numerical model can be used to predict different scenarios for piping erosion for particular soil mixtures.

Following conclusions may be drawn from the results of the numerical model study:

- Numerical model using Exner equation is developed to describe the development of erosion with time and to analyze effect of different parameters on the internal erosion process, e.g., the upstream and downstream slopes, the crest width, the initial upstream water depth and the initial piping diameter.
- Effect of changing the upstream slope on the depth erosion is higher than that of the downstream slope.
- Increasing the crest width causes a decrease in the erosion depth.

7.3 Recommendations

The following are recommendations in future investigations

- Experiments may be conducted with more soil mixtures chosen from USDA soil chart to get more data and see the effect of various soil mixtures.
- The location of piping may be changed along the vertical plane and the bed plane to see details of erosion pattern.
- Experiments may be conducted to study the effect of the variation of discharge and water depth on different soil mixtures.

References

Alamdari, N. Z., M. Banihashemi, and A. Mirghasemi (2012). A numerical modeling of piping phenomenon in earth dams. *World Academy of Science, Engineering and Technology*, 45–47.

Arulanandan, K. and E. B. Perry (1983). Erosion in relation to filter design criteria in earth dams. *Journal of Geotechnical Engineering 109*(5), 682–698.

Awal, R., H. Nakagawa, M. Fujita, K. Kawaike, Y. BABA, and H. ZHANG (2011). Study on piping failure of natural dam. *Disaster Prevention Research Institute Annuals. B 54*(B), 539–547.

Balloffet, A. and M. L. Scheffler (1982). Numerical analysis of the teton dam failure flood.

Bendahmane, F., D. Marot, and A. Alexis (2008). Experimental parametric study of suffusion and backward erosion. *Journal of geotechnical and geoenvironmental engineering 134*(1), 57–67.

Bonelli, S., N. Benahmed, et al. (2010). Piping flow erosion in water retaining structures: inferring erosion rates from hole erosion tests and quantifying the failure time. In *IECS 2010, 8th ICOLD European Club Symposium Dam Safety-Sustainability in a Changing Environment*.

Chapuis, R. P. (1986). Quantitative measurement of the scour resistance of natural solid clays. *Canadian Geotechnical Journal 23*(2), 132–141.

Chapuis, R. P. and T. Gatien (1986). An improved rotating cylinder technique for quantitative measurements of the scour resistance of clays. *Canadian Geotechnical Journal 23*(1), 83–87.

Fell, R., C. F. Wan, J. Cyganiewicz, and M. Foster (2003). Time for development of internal erosion and piping in embankment dams. *Journal of geotechnical and geoenvironmental engineering 129*(4), 307–314.

Foster, M., R. Fell, and M. Spannagle (2000a). A method for assessing the relative likelihood of failure of embankment dams by piping. *Canadian Geotechnical Journal 37*(5), 1025–1061.

Foster, M., R. Fell, and M. Spannagle (2000b). The statistics of embankment dam failures and accidents. *Canadian Geotechnical Journal 37*(5), 1000–1024.

Gonzalez, R. C., R. E. Woods, and S. L. Eddins (2009). *Digital image processing using MATLAB*, Volume 2. Gatesmark Publishing Tennessee.

Hanson, G. (1991). Development of a jet index to characterize erosion resistance of soils in earthen spillways. *Transactions of the ASAE 34*.

Hanson, G. and K. Robinson (1993). The influence of soil moisture and compaction on spillway erosion. *Transactions of the ASAE 36*.

Hanson, G., R. Tejral, S. Hunt, and D. Temple (2010). Internal erosion and impact of erosion resistance. In *Proceedings of the 30th US Society on Dams Annual Meeting and Conference*, pp. 773–784.

Hanson, G., T. Wahl, D. Temple, S. Hunt, and R. Tejral (2010). Erodibility characteristics of embankment materials. In *State Dam Safety Officials Association Proceedings*.

Jähne, B. (1997). *Image processing for scientific applications*. CRC press Boca Raton.

Lachouette, D., F. Golay, and S. Bonelli (2008). One-dimensional modeling of piping flow erosion. *Comptes Rendus Mecanique 336*(9), 731–736.

Maranha das Neves, E. (1989). Śanalysis of crack erosion in dam cores. the crack erosion test. *de Mello Volume, Sao Paulo, Brazil*, 284–298.

Marot, D., P.-L. Regazzoni, and T. Wahl (2011). Energy-based method for providing soil surface erodibility rankings. *Journal of Geotechnical and Geoenvironmental Engineering 137*(12), 1290–1293.

Meyer-Peter, E. and R. Müller (1948). Formulas for bed-load transport. In *Proceedings of the 2nd Meeting of the International Association for Hydraulic Structures Research*, pp. 39–64. Stockholm.

Morris, M., M. Hassan, and K. Vaskinn (2007). Breach formation: Field test and laboratory experiments. *Journal of Hydraulic Research 45*(sup1), 9–17.

Ojha, C., V. Singh, and D. Adrian (2001). Influence of porosity on piping models of levee failure. *Journal of geotechnical and geoenvironmental engineering 127*(12), 1071–1074.

Reddi, L. N., I.-M. Lee, and M. V. Bonala (2000). Comparison of internal and surface erosion using flow pump tests on a sand-kaolinite mixture. *ASTM geotechnical testing journal 23*(1), 116–122.

Regazzoni, P., D. Marot, J. Courivaud, G. Hanson, and T. Wahl (2008). Soil erodibility: A comparision between the jet erosion test and the hole erosion test. In *Proceeding of the inaugural international conference of the engineering mechanics institute, Minneapolis, Minnesota*, pp. 1–7.

Richards, K. S. and K. R. Reddy (2010). True triaxial piping test apparatus for evaluation of piping potential in earth structures. *Geotechnical Testing 33*.

Shaikh, A., J. F. Ruff, and S. R. Abt (1988). Erosion rate of compacted na-montmorillonite soils. *Journal of geotechnical engineering 114*(3), 296–305.

van Beek, V., H. de Bruijn, J. Knoeff, A. Bezuijen, and U. Förster (2010). Levee failure due to piping: A full-scale experiment. In *Scour and Erosion*, pp. 283–292. ASCE.

Vaskinn, K. A., A. Løvoll, K. Höeg, M. Morris, G. Hanson, and M. Hassan (2004). Physical modeling of breach formation: Large scale field tests. In *Proc. of the Annual Conf. of the ASDSO*.

Wahl, T. (2010). A comparision of the hole erosion test and jet erosion test. In *Proceeding of the Joint Federal Interagency Confernce on Sedimentation and Hydrologic Modeling, Las Vegas, NV*, pp. 1–11.

Wan, C. and R. Fell (2004a). Investigation of rate of erosion of soils in embankment dams. *Journal of Geotechnical and Geoenvironmental Engineering 130*(4), 373–380.

Wan, C. F. and R. Fell (2004b). Laboratory tests on the rate of piping erosion of soils in embankment dams. *ASTM geotechnical testing journal 27*(3), 295–303.

Zhou, J. and K.-m. Zhou (2010). 3d modeling of piping mechanism using distinct element method. In *Soil Behavior and Geo-Micromechanics*, pp. 227–233. ASCE.